HHS Public Access

Author manuscript

J Neurosci Methods. Author manuscript; available in PMC 2021 November 01.

Published in final edited form as:

J Neurosci Methods. 2020 November 01; 345: 108859. doi:10.1016/j.jneumeth.2020.108859.

Using rAAV2-retro in rhesus macaques: Promise and caveats for circuit manipulation

Adriana K. Cushnie[a,*], **Hala G. El-Nahal**[b,*], **Martin O. Bohlen**[b], **Paul J. May**[c], **Michele A. Basso**[d], **Piercesare Grimaldi**[d], **Maya Zhe Wang**[a], **Ezequiel Marron Fernandez de Velasco**[e], **Marc A. Sommer**[b,f,g], **Sarah R. Heilbronner**[a]

[a]Department of Neuroscience, University of Minnesota, Minneapolis, MN 55455

[b]Department of Biomedical Engineering, Duke University, Durham, NC 27708

[c]Department of Neurobiology and Anatomical Sciences, University of Mississippi Medical Center, Jackson, 39216

[d]Fuster Laboratory of Cognitive Neuroscience, Department of Psychiatry and Biobehavioral Sciences and Neurobiology, and Jane and Terry Semel Institute for Neuroscience and Human Behavior, David Geffen School of Medicine, Univ. of California Los Angeles, Los Angeles, CA USA 90095

[e]Department of Pharmacology, University of Minnesota, Minneapolis, MN 55455

[f]Department of Neurobiology, Duke University School of Medicine, Durham, NC 27708

[g]Center for Cognitive Neuroscience, Duke University, Durham, NC 27708

Abstract

Background—Recent genetic technologies such as opto- and chemogenetics allow for the manipulation of brain circuits with unprecedented precision. Most studies employing these techniques have been undertaken in rodents, but a more human-homologous model for studying the brain is the nonhuman primate (NHP). Optimizing viral delivery of transgenes encoding actuator proteins could revolutionize the way we study neuronal circuits in NHPs.

Correspondence: Sarah R. Heilbronner, PhD, University of Minnesota, Department of Neuroscience, 2-164 Jackson Hall, 321 Church St SE, Minneapolis, MN 55455, heilb028@umn.edu, 612-626-4429, heilbronnerlab.umn.edu.

*These authors contributed equally

Author Contributions

Adriana K. Cushnie: Conceptualization, Methodology, Validation, Investigation, Writing – Original Draft, Visualization, Funding Acquisition **Hala G. El-Nahal:** Conceptualization, Methodology, Validation, Investigation, Writing – Original Draft, Visualization **Martin O. Bohlen:** Conceptualization, Methodology, Validation, Investigation, Writing – Review & Editing, Visualization **Paul J. May:** Conceptualization, Methodology, Validation, Investigation, Writing – Review & Editing, Funding Acquisition **Michele A. Basso:** Conceptualization, Methodology, Investigation, Writing – Review & Editing, Funding Acquisition **Piercesare Grimaldi:** Methodology, Investigation **Maya Zhe Wang:** Methodology, Investigation, Writing – Review & Editing **Ezequiel Marron Fernandez de Velasco:** Methodology, Validation, Investigation, Resources, Writing – Review & Editing, **Marc A. Sommer:** Conceptualization, Methodology, Validation, Investigation, Writing – Review & Editing, Supervision, Funding Acquisition **Sarah R. Heilbronner:** Conceptualization, Methodology, Validation, Investigation, Writing – Original Draft, Visualization, Supervision, Funding Acquisition

Declarations of interest: None.

New Method—rAAV2-retro, a popular new capsid variant, produces robust retrograde labeling in rodents. Whether rAAV2-retro's highly efficient retrograde transport would translate to NHPs was unknown. Here, we characterized the anatomical distribution of labeling following injections of rAAV2-retro encoding opsins or DREADDs in the cortico-basal ganglia and oculomotor circuits of rhesus macaques.

Results—rAAV2-retro injections in striatum, frontal eye field, and superior colliculus produced local labeling at injection sites and robust retrograde labeling in many afferent regions. In every case, however, a few brain regions with well-established projections to the injected structure lacked retrogradely labeled cells. We also observed robust terminal field labeling in downstream structures.

Comparison with Existing Method(s)—Patterns of labeling were similar to those obtained with traditional tract-tracers, except for some afferent labeling that was noticeably absent.

Conclusions—rAAV2-retro promises to be useful for circuit manipulation via retrograde transduction in NHPs, but caveats were revealed by our findings. Some afferently connected regions lacked retrogradely labeled cells, showed robust axon terminal labeling, or both. This highlights the importance of anatomically characterizing rAAV2-retro's expression in target circuits in NHPs before moving to manipulation studies.

Keywords

nonhuman primate; rAAV2-retro; DREADDs; optogenetics; chemogenetics

INTRODUCTION

Genetic technologies, like optogenetics and chemogenetics, have revolutionized neuroscience research in small animal models. However, translation of these technologies to rhesus macaques – an animal model with considerable neural homology to humans – has been slow. Transgenic technology in small animal models plays a critical role in the successful *in vivo* expression of exogenous actuator proteins (e.g., opsins or chemogenetic receptors) in target neuronal populations, but transgenic rhesus macaques are impractical and not widely available. Thus, researchers must resort to using replication-deficient viral vectors to deliver transgenes to target neuronal populations in rhesus macaques. Achieving robust pathway-selective expression of a transgene in nonhuman primates (NHPs) via viral delivery can often be challenging due to poor infection rates (Upright et al., 2018) and weak spread of viral vectors from injection sites (for full reviews of the challenges associated with optogenetics and chemogenetics in NHPs, see El-Shamayleh et al., 2016; El-Shamayleh and Horwitz, 2019; Galvan et al., 2017, 2018).

Nevertheless, progress is being made. Studies have employed anterograde pathway-selective optogenetics in NHPs by injecting an opsin-encoding virus that is preferentially internalized at cell bodies in one region and illuminating the axon terminals of infected neurons downstream. Inoue and colleagues (2015) injected frontal eye field (FEF) then optically stimulated axon terminals of FEF neurons in superior colliculus (SC) (Inoue et al., 2015). Galvan and colleagues (2016) injected the primary motor and premotor cortices then optically stimulated the axon terminals of infected cortical neurons in the thalamus (Galvan

et al., 2016). Nurminen and colleagues (2018) injected the secondary visual area then optically inhibited axon terminals in primary visual cortex (Nurminen et al., 2018). Yazdan-Shahmorad and colleagues (2018) injected the motor thalamus then optically stimulated thalamo-cortical axons in the primary motor cortex (Yazdan-Shahmorad et al., 2018). Maeda and colleagues (2020) injected the amygdala then optically stimulated amygdalo-nigral axon terminals (Maeda et al., 2020).

Retrograde pathway-selective opto- or chemogenetics involves injecting a virus that is preferentially internalized at axon terminals at the injection site, then retrogradely transported to upstream cell bodies, allowing for optical or ligand-mediated manipulation of a pathway. Retrograde pathway-selective manipulation affords the powerful ability to compare contributions of multiple inputs to a single brain area. Senova and colleagues (2018) combined retrograde pathway-selective optogenetics with diffusion-weighted magnetic resonance imaging tractography to characterize the motor cortico-subthalamic pathway. They injected retrogradely transported opsin-encoding viral constructs into the subthalamic nucleus then optically stimulated cell bodies of cortico-subthalamic neurons (Senova et al., 2018). Other NHP studies have used retrograde viruses for pathway-selective neurotoxin expression (Inoue et al., 2012; Kinoshita et al., 2019, 2012; Takada et al., 2013; Tohyama et al., 2017). In addition, numerous anatomical studies have characterized a range of retrograde viruses in NHPs (Kato et al., 2011a., 2011b; Masamizu et al., 2011; Oguchi et al., 2015; Tanabe et al., 2017; Tanabe et al., 2019; Weiss et al., 2020). Retrogradely transported viruses include canine adenovirus type 2 (Soudais et al., 2001), herpes simplex virus (Jin Bak et al., 1977), rabies virus (Tsiang, 1979), and pseudotyped lentiviral vectors such as HiRet and EIAV (Kato et al., 2011a.; Senova et al., 2018). These viruses can be neurotoxic, however, and some infect glia in addition to neurons (Bohlen et al., 2019; Tanabe et al., 2019; Callaway and Luo, 2015; Ginger et al., 2013; Marconi et al., 2008; Schnell et al., 2010).

In contrast, recombinant adeno-associated viruses (rAAVs) are relatively safe and commonly used in gene therapy and research. AAVs are non-enveloped, single-stranded DNA viruses (Aponte-Ubillus et al., 2018). rAAVs are produced by removing the viral DNA from wild-type AAVs and replacing the coding and non-coding DNA regions with an expression cassette encoding a transgenic protein of interest (Büeler, 1999; Samulski et al., 1989). These modifications render rAAVs replication deficient. rAAVs are particularly suitable for transgene delivery to the brain because they can transduce post-mitotic tissue, and their genome remains episomal (Choi et al., 2006; Naso et al., 2017). Moreover, they produce long term, stable expression of transgenes, while being minimally immunogenic (Aponte-Ubillus et al., 2018; Kaspar et al., 2002; Nassi et al., 2015). Thus, rAAVs have been used to deliver a range of transgenes in clinical trials for neurological disorders (Monahan and Samulski, 2000; Ojala et al., 2015; Simonelli et al., 2010). Until recently, rAAVs produced limited retrograde transport (Aschauer et al., 2013; Castle et al., 2014; Hadaczek et al., 2016; Masamizu et al., 2011; McFarland et al., 2009; Salegio et al., 2013; San Sebastian et al., 2013; Taymans et al., 2007; Towne et al., 2010). In NHP opto- and chemogenetics studies, AAVs primarily have been used to manipulate neural activity local to the injection site (Acker et al., 2016; Afraz et al., 2015; Cavanaugh et al., 2012; Dai et al., 2014; El-Shamayleh et al., 2017; Fetsch et al., 2018; Grayson et al., 2016; Ju et al., 2018; Klein et al.,

2016; Lu et al., 2015; May et al., 2014; Nagai et al., 2016; Nakamichi et al., 2019; Raper et al., 2019; Stauffer et al., 2016; Tamura et al., 2017; Upright et al., 2018; Yazdan-Shahmorad et al., 2016). However, a new rAAV variant—rAAV2-retro—developed through *in vivo* directed evolution (Tervo et al., 2016) has gained recent popularity because of its highly efficient retrograde transport in rodents (Birdsong et al., 2019; Hong and Heo, 2020).

Motivated by the quest for a non-toxic retrograde virus that reliably and robustly expresses exogenous actuator proteins in rhesus macaques, we sought to determine if rAAV2-retro's efficient retrograde transport would translate to monkeys. Therefore, we injected rAAV2-retro into rhesus macaque striatal and oculomotor structures, then anatomically characterized their transgene expression. These structures were chosen because their connectivity has been studied extensively, allowing for validation. Following rAAV2-retro injections, we observed extensive retrograde labeling in many regions with afferent connections to the injection sites. The observed degree of labeling would likely be sufficient for circuit manipulation. Although rAAV2-retro produced robust retrograde labeling, it did not retrogradely label *all* expected regions. Moreover, rAAV2-retro strongly labeled axon terminals in many areas that receive direct projections from the injection site. These caveats are critical to consider when designing rhesus macaque opto- and chemogenetic experiments, and they suggest that anatomical characterization of rAAV2-retro in regions of interest should precede physiological and behavioral experiments.

MATERIALS AND METHODS

One female and three male (7–20yrs; 7–14kg; Case 1–5, Table 1) rhesus macaques (*Macaca mulatta*) were used in this study. Cases 3 and 4 are separate injections in the same animal. All methods are in accordance with the NIH *Guidelines for Animal Care and Use* and were independently approved by the Institutional Animal Care and Use Committees at the University of Minnesota, Duke University, and the University of California, Los Angeles. Prior to this study, the subject for Case 1 participated in electrophysiological and psychophysical experiments (Grimaldi et al., 2018; Odegaard et al., 2018), the subject for Case 2 participated in transcranial electric and magnetic stimulation studies (Lee et al., 2017, 2015; Peterchev et al., 2015, 2008), and the subjects for Cases 2–5 received additional viral injections as part of different studies (unpublished data) that were not included in the current analyses.

Viral Vectors

Table 1 lists all viral vectors used in the study. Viral vector solutions were shipped on dry ice and, upon receipt, immediately placed in a −80°C freezer. In some cases, the viral vector solution was allowed to thaw briefly for aliquoting. Aliquots were placed in pre-chilled non-stick micro-centrifuge tubes (VWR International, Radnor, PA) and stored in a −80°C freezer until injection day. On injection day, viral solutions were removed from the −80°C freezer and stored in a cooler filled with dry ice. Immediately before use, the vials were allowed to thaw on wet ice then briefly centrifuged and drawn into a 10 or 25μl Hamilton syringe. A new aliquot of AAV was used for each procedure and surplus virus was discarded in bleach.

Viral Injections

Implanted chamber injections—For a single case (Case 1), an existing chamber implant allowed intracranial access without surgery. The injection site was identified by electrophysiological recordings of SC neurons discharging maximally for horizontal contraversive saccades of 10–15° amplitude above the horizontal meridian, based on previous electrophysiological recordings (Grimaldi et al., 2018; Odegaard et al., 2018). A 10μl Hamilton syringe was used to inject a total of 9μl at 0.1μl/min, divided between 3 locations within the SC. At each location, 1μl injections were made at 2, 1.5, and 1mm from the surface of the SC.

Stereotaxic injections—For 4 cases (Cases 2–5), a surgical procedure was used to inject viral constructs intracranially. For prophylactic measures against inflammation, animals received a dexamethasone injection (2.0 mg/kg, IM) one day prior to surgery, and on the surgery day (Case 2) or diphenhydramine (2.0–4.0 mg/kg, IM) on the surgery day only (Cases 3–5). Before transport to the surgical suite, animals were sedated with ketamine hydrochloride (3.0 mg/kg, IM) and dexdomitor (0.075 mg/kg, IM) (Case 2) or ketamine (10.0mg/kg, IM), midazolam (0.25mg/kg, IM), atropine (0.04mg/kg, IM) and ondansetron (0.15mg/kg, SQ) (Cases 3–5). Once in the surgical suite, animals were intubated, and an anesthetic plane was maintained for the duration of surgery using 1–3% isoflurane/oxygen mix. Some animals (Cases 3–5) received ceftriaxone (100.0mg/kg, IM) and buprenorphine (.01mg/kg, IM/IV/SQ) at the start of surgery. Buprenorphine was then administered every 4–6 hrs during the surgery (which lasted 6–8 hrs) and once the morning after (Cases 3–5).

All surgical procedures were carried out under aseptic conditions. Incision sites were disinfected using betadine and chlorhexidine scrubs, followed by 100% ethanol. During surgery, vital signs were monitored and maintained within normal limits by a trained veterinary technician. Before every incision and after final suturing, a cutaneous injection of 0.25% bupivacaine (0.5–1.0 ml/<4mg) was administered along the incision site and mannitol (0.25–2.5g/kg, IV) was administered before the craniotomy bone plate was removed (Case 3–5).

At the start of surgery, the animal was placed into a stereotaxic apparatus (Kopf Instruments, Tujunga, CA). A midline incision was made, and the muscle and fascia were displaced to expose the skull. A craniotomy was performed, and dura was removed. For Case 2, the FEF was identified by visualization of the dorsal superior- and ventral inferior-arcuate sulci, with the arcuate spur lying posteriorly and the principal sulcus lying anteriorly. A 10μl Hamilton microsyringe was then held in a micromanipulator at a 45° angle with its tip at the cortical surface, pointing toward the midline. After getting a surface measurement, the needle was advanced to 5 mm below the cortical surface. At this location, 2μl of rAAV2-retro-CAG-GFP were pressure injected and allowed to diffuse from the injection site for 5 mins. Subsequently, the syringe was drawn up 1 mm and a 1μl injection was made, followed by a second 5-min wait period. This procedure was replicated at 6 different sites along the genu of the arcuate sulcus. Injections were performed at a rate of 1μl /min. For Cases 3–5, surface and midline measurements were used to calculate the coordinates of striatal targets that were pre-established based on Paxinos et al., (2000). A 10μl Hamilton microsyringe held in a

motorized micromanipulator was lowered into targets. Case 3 received 25μl of rAAV2-retro-CaMKII-hM4Di-mCherry in the medial caudate (AP 26.5, ML 3.5, DV 16.0), Case 4 received 25μl of rAAV2-retro-hSyn-hM4Di-HA distributed across two sites (dorsal-ventrally) within the lateral putamen (AP 19.5, ML 14.0, DV 21.0/23.0), and Case 5 received 18μl of rAAV2-CaMKII-hM4Di-mCherry distributed across 2 sites (dorsal-ventrally) in the central striatum (AP 23.5, ML 8.0, DV 18/20.3). Viruses were infused at a rate of 0.5–1.0μl/min. The Hamilton syringe remained *in situ* for 10 mins at the end of each infusion and between sites. For all cases, after completion of injections, the syringe was withdrawn, and the bone flap was replaced and held in place with gel foam. Next, the muscle, followed by the skin, was sutured and anesthesia was discontinued. The animal was extubated, returned to its home cage, and monitored for recovery until normal behavior was observed. For postoperative analgesia, one animal received one dose of buprenorphine SR (0.2mg/kg, IM) and 1.0mg/kg of dexamethasone for three days post-op, then 0.5 mg/kg of dexamethasone every other day for an additional week (Case 2). Others received meloxicam (0.1mg/kg, PO) for 72hrs post-surgery and the antibiotic ceftiofur (5.0mg/kg; SQ/IM) once daily for 7 days as a preventative measure (Cases 3–5).

Histology and Microscopy

Animal survival times post-surgery ranged between 28–264 days (Table 1). Before euthanasia, animals were sedated with ketamine hydrochloride (3.0 mg/kg, IM) then deeply anesthetized with sodium pentobarbital (50.0 mg/kg, IP). Once areflexic, animals were transcardially perfused with 1–4L of chilled 0.1M, pH 7.4 phosphate buffered saline (PBS), followed by 4L of 4% paraformaldehyde in 0.1M, pH 7.4 PBS.

For Cases 1 and 2, the brain was blocked in the frontal plane using a stereotaxic apparatus then post-fixed in 4% paraformaldehyde in 0.1M, pH 7.4 PBS at 4°C for 24–48 hrs. Blocks were then cryoprotected in 30% sucrose at 4°C. Afterwards, they were cut into 50μm (Case 1) or 75μm (Case 2) coronal sections using a freezing stage sliding microtome (American Optical Company, Buffalo, NY) and stored in PBS at 4°C. For processing, sections were divided into 6 rostral to caudal series, with ~300μm (Case 1) or ~450 μm (Case 2) between adjacent sections in the series. For Cases 3–5, whole brains were postfixed overnight and cryoprotected in increasing gradients of sucrose (10, 20, and 30%). Next, they were blocked in the frontal plane, and serial sections of 50μm were cut on a freezing microtome and stored in cryoprotectant solution.

Processing for fluorescence microscopy

Case 1: To observe virus-driven epifluorescence without immunological amplification, sections were simply mounted on gelatinized (10% gelatin) glass slides and allowed to dry overnight. Next, they were dehydrated in a gradient of alcohol baths (70%, 95%, 100% - 2 mins in each) and coverslipped using Cytoseal 60 (Thermo Fisher Scientific).

For immunofluorescence amplification, sections were placed in immunoblocking serum consisting of 1% bovine serum albumin in 0.1 % Triton X-100 in PBS for 2 hrs at room temperature. After rinsing, they were incubated with a rabbit anti-GFP antibody in PBS (1:200; Abcam #5450) overnight at 4°C. The next day they were rinsed again and placed in a

secondary antibody solution consisting of 1:385 donkey anti-rabbit antibody conjugated to Alexa Fluor 488 (Jackson ImmunoResearch #705–545-147) in 2% normal donkey serum in PBS for 2 hrs at room temperature.

Immunohistochemical processing for light microscopy

Case 2: Serial free-floating sections (one in six) were washed with 0.1M, pH 7.4 PBS then incubated in 0.3% H_2O_2 in 0.1M, pH 7.4 PBS to block endogenous peroxidase activity. Sections were washed in PBS then moved to a 0.25% solution of Triton X-100 in PBS. Next, sections were transferred to a 1% BSA/0.25% Triton X-100 in PBS solution.

For visualization of GFP expression, sections were incubated in biotinylated goat anti-GFP antibody (~ 1:200; Rockland 600–106-215) in a 1% BSA/0.25% Triton X-100 in PBS solution for 1–3 hrs at room temperature, then ~48 hrs at 4°C. Next, sections were washed with PBS then incubated in biotinylated rabbit anti-goat IgG secondary antibody (Vector Laboratories, PK6105) for 1.5 hrs at room temperature. Sections were then transferred to an avidin-biotin-horseradish peroxidase complex (ABC) solution (Vector Laboratories, PK6105) for 1 hr at room temperature. Following another 15 min PBS wash, sections were placed in 0.5% diaminobenzidine (DAB)/0.01% cobalt chloride/0.01% nickel ammonium sulfate in PBS solution for 20 mins. Subsequently, 0.3% H_2O_2 was added and allowed to react with the DAB for 15–30 mins. Afterwards, a final PBS wash was done. Sections were then mounted on gelatinized glass slides and left to air dry overnight.

Dry mounted sections were stained with thionin, then dehydrated in a gradient of alcohol baths and coverslipped using Cytoseal 60. Sections were then air dried and stored at room temperature.

Cases 3–5: Serial free-floating sections (one in eight) were washed in 0.1M PO_4- TX, then incubated in 0.3% H_2O_2 to block endogenous peroxidase activity. Sections were incubated in primary anti-mCherry antibody (1:1000; Abcam AB167453) and anti-HA antibody (1:400; Abcam Ab1549585) in 10% NGS and 0.3% Triton X-100 (Sigma-Aldrich) in PO_4 for 4 days at 4°C. After extensive washing, the tissue was incubated in a biotinylated secondary antibody followed by incubation in ABC solution (Vectastain ABC kit, Vector Laboratories). Immunoreactivity was visualized using standard DAB procedures. Staining was intensified by incubating the tissue for 5–15 s in a solution of 0.05% DAB tetrahydrochloride and 0.01% H_2O_2. Sections were mounted onto gel-coated slides, dehydrated, defatted in xylene, and coverslipped with Permount.

Microscopy—Transgene expression was visualized and charted using a Nikon Eclipse E600 microscope equipped with a DS-Ri1 digital camera (Case 1), a Zeiss AxioImager 2 microscope equipped with either an Axiocam 506 color camera (Case 2) or a Lumina HR camera (Cases 3–5), or a Bausch & Lomb microprojection microscope (Case 2). StereoInvestigator and NeuroLucida Softwares (MBF Biosciences, Inc) were used to chart labeling in some structures (Cases 3–5). Brightfield, darkfield, and fluorescence microscopy were employed. Digital photomicrographs were obtained using Nikon Elements software (Case 1), Zeiss Zen software (Case 2) or NeuroLucida Software (Case 3–5). Photomicrographs were adjusted for brightness and contrast in Adobe Photoshop.

RESULTS

Overview

Following injections into key oculomotor and striatal structures, substantial retrograde labeling was observed. However, this was not true for all established afferent projections to the injected structures. In addition, extensive terminal field labeling was consistently observed. Finally, no "false positives," or signs of multisynaptic labeling were detected. An exhaustive list of the labeling or lack of labeling observed in all areas connected to each injected structure is beyond the scope of this paper. Therefore, the following sections focus on areas known to have strong, consistent connections to the injected structures, or connections that have been of particular functional interest to the neuroscience community.

Substantial retrograde labeling

Case 1: Superior colliculus (SC)—Case 1 consisted of an injection of rAAV2-retro-hSyn-hChR2(H134R)-EYFP into the SC (Figure 1). We examined the pattern of virus-driven epifluorescence and compared it to labeling seen using immunofluorescence intensification. All heavily labeled structures in the intensified material showed fluorescent label in the non-intensified material. However, the degree of dendritic labeling and the number of labeled cells was improved by the intensification, and lightly labeled structures in the intensified material sometimes lacked label in material that was not intensified.

Following rAAV2-retro injections in SC, retrogradely labeled neurons were observed in the FEF ipsilateral to the injected SC (Figure 2A–B). Thus, an important corticocollicular circuit, previously demonstrated by classical tracers (Fries, 1984), is readily evident in this material. There was additional cortical labeling in the rest of area 8, area 6, anterior cingulate cortex (area 24), primary motor cortex, and the ventrolateral prefrontal cortex (area 45). Subcortically, we observed retrogradely labeled cells in a number of structures (not illustrated); most notably: the contralateral intermediate gray layer of the SC, the peri-interstitial nucleus of Cajal portion of the mesencephalic reticular formation (piMRF), the central mesencephalic reticular formation (cMRF) and the peri-parabigeminal nucleus of the midbrain, the reticular formation and parabrachial nuclei of the pons, and the vestibular and trigeminal sensory nuclei of the medulla. Labeling was particularly prominent in the deep cerebellar nuclei. All of these connections have been reported previously following injections of traditional retrograde tracers into the SC of NHPs (Fries, 1984; Leichnetz et al., 1981; May et al., 1990; May, 2006).

Case 2: Frontal eye field (FEF)—Case 2 consisted of an injection of rAAV2-retro-CAG-eGFP into the FEF (Figure 1). As expected, retrograde labeling could be observed in the FEF contralateral to the injection site (Figure 2C). Additional cortical labeling was observed ipsilaterally in other portions of area 8, anterior cingulate cortex (area 24), premotor cortex (area 6), and the dorsal and ventral banks of the superior temporal sulcus. There was also subcortical labeling. Retrogradely labeled neurons were present in the claustrum (Figure 2D) and in the basolateral nucleus of the amygdala (not illustrated). All of these connections have been previously reported following injections of traditional retrograde tracers into the FEF (Leichnetz, 1982; Leichnetz and Goldberg, 1988).

Case 3: Medial caudate nucleus (mCd)—Case 3 consisted of an injection of rAAV2-retroCaMKII-hM4Di-mCherry into the mCd, reaching to the head of the caudate nucleus (Figure 1). Consistent with prior reports, the strongest retrograde cortical labeling was observed in the frontal lobe (Figure 3A–D), with particularly dense labeling of cell populations in the dorsal and pregenual anterior cingulate cortex (areas 24 and 32), dorsal frontal cortex (areas 9/32, 8/32, 9, 8, and rostral portions of areas 6 and 6/32), the ventromedial prefrontal cortex (area 14), and the frontal pole (area 10). Significant, but less dense labeling, could also be observed in dorsolateral prefrontal cortex (areas 9/46, 46V, 46D), ventrolateral prefrontal cortex (areas 45 and 47), caudal orbitofrontal cortex (area 13) and ventromedial prefrontal cortex (area 25). Outside of the frontal lobe, labeling was less dense, but included the amygdala, hippocampus, entorhinal cortex, posterior cingulate cortex (areas 23 and 30), and parietal area PG. No labeling was expected or observed in primary sensory or motor cortices. Subcortically, there was light labeling in the anterior thalamus and claustrum, consistent with prior work (Arikuni and Kubota, 1985). We did not expect to see retrograde labeling in the pallidum for this case because CaMKII (the promoter used) is not expressed in this brain region (Benson et al., 1991; Wang et al., 2013). All of these projections are consistent with prior studies demonstrating cortical projections to the mCd with conventional tracers (Ferry et al., 2000; Haber et al., 2006; Takada et al., 2001; Yeterian and Van Hoesen, 1978).

Case 4: Lateral putamen (lPut)—Case 4 consisted of an injection of rAAV2retro-hSyn-hM4Di-HA into the lPut, with some potential contamination in the ventral claustrum and adjoining white matter (Figure 1). This case showed a very different pattern of cortical labeling than Case 3. There was significant retrograde labeling in primary somatosensory cortex (Figure 3E&G), and lighter labeling in primary motor cortex, area 6, area 6/32, area 24, area 8, and the ventrolateral prefrontal cortex (areas 45 and 44). All of these projections are consistent with prior studies demonstrating cortical projections to the lPut with conventional tracers (Kita et al., 1999; Künzle, 1977; Takada et al., 2001).

Case 5: Central striatum (cStr)—Case 5 consisted of an injection of rAAV2retro-CaMKI-hM4Di-mCherry into the dorsal cStr, spanning portions of both the lateral caudate and medial putamen (Figure 1). We observed less labeling in this case than in the others. This is probably because much of the injection volume wound up in the white matter of the internal capsule. Nevertheless, there was significant retrograde labeling in the dorsal frontal cortex (areas 10, 46, 9, 8, 6, 6/32) (Figure 3F), the dorsal anterior cingulate cortex (area 24), the ventrolateral prefrontal cortex (areas 47 and 45), and the central orbitofrontal cortex (area 11). There were scattered cells visible in the thalamus. There was very little label outside of these areas. All of these projections are consistent with prior studies demonstrating cortical projections to the dorsal cStr with conventional tracers (Haber et al., 2006; Takada et al., 2001; Yeterian and Van Hoesen, 1978).

False negatives in retrograde labeling

There were several instances in which we did not observe the expected pattern of afferent labeling.

Case 1: SC—We anticipated retrograde labeling in the substantia nigra pars reticulata (May, 2006) and the zona incerta (Basso and May, 2017), two major sources of GABAergic input to the SC. However, there were no cells visible in the substantia nigra pars reticulata (Figure 4A) or the zona incerta (not illustrated).

Case 2: FEF—We expected strong retrograde labeling in the caudal bank of the intraparietal sulcus (Leichnetz and Goldberg, 1988), but did not observe any labeling there. In addition, we anticipated extensive retrograde labeling in the thalamus (Huerta et al., 1986; Leichnetz and Goldberg, 1988), particularly in the mediodorsal nucleus and the pulvinar, which are the primary sources of ascending input to the FEF. However, retrogradely labeled cells were not present in any thalamic nuclei. Lastly, we expected, but did not find, retrograde labeling in the locus coeruleus (Leichnetz and Goldberg, 1988).

Case 3: mCd—The most significant false negative in this case was the lack of retrogradely labeled cells in the substantia nigra pars compacta.

Case 4: lPut—Because the promoter used in this case was hSyn (rather than CaMKII), we *did* expect, but did not observe, substantial retrograde labeling in the internal and external segments of the globus pallidus. Additionally, there were no labeled cells in any portion of the substantia nigra.

Case 5: cStr—As in Case 3, we expected, but did not observe, retrograde labeling in the substantia nigra pars compacta.

Downstream axon terminal labeling

Case 1: SC—The pattern of terminal labeling observed in the brainstem following SC injections (not illustrated) was very similar to that observed previously with conventional tracers (Harting, 1977; Basso and May, 2017). In particular, terminal fields were observed in the midbrain, pontine and medullary reticular formation, as well as in the supraoculomotor area, nucleus reticularis tegmenti pontis and inferior olive. Ascending pathways were also labeled. For example, extensive terminal field labeling, with numerous axonal boutons, could be observed in the paralamellar mediodorsal nucleus of the thalamus (Figure 4B–C). This labeling was visually compared with results from conventional anterograde tract-tracers placed in the SC and found to be topographically similar (Figure 4C; Harting et al., 1980; May, 2006; Basso and May, 2017).

Case 2: FEF—We observed axon terminal labeling in many downstream structures following FEF injections. Extensive terminal field labeling was observed in the mediodorsal nucleus of the thalamus (Figure 4D), as well as the medial pulvinar nucleus (not illustrated). We also saw axons terminating in the caudate, putamen, subthalamic nucleus. Additional subcortical labeling was observed in the zona incerta, prerubral field, rostral interstitial nucleus of MLF (riMLF), interstitial nucleus of Cajal, nucleus of Darkschewitsch and periaqueductal gray. An extensive plexus of labeled axons was present in the intermediate gray layer of the SC (Figure 4E). This pattern of terminal labeling is consistent with results

from classical anterograde tract-tracer studies (Huerta et al., 1986; Leichnetz and Goldberg, 1988; Stanton et al., 1988A&B).

Case 3: mCd—Particularly dense terminal field labeling was observed in both the internal and external segments of the pallidum (Figure 5A). This labeling was located in the rostral dorsomedial portions of both segments, in keeping with the highly topographic nature of the striato-pallidal projection (Heilbronner et al., 2018). Notably, this outcome cannot be due to misconstruing labeled dendrites as axons because the CaMKII promoter is not expressed in the pallidum (Benson et al., 1991), so we do not see retrogradely labeled cells there. There were also densely terminating axons in the substantia nigra, likely involving both the pars compacta and pars reticulata (Figure 5B).

Case 4: lPut—Similar to Case 3, particularly dense terminal field labeling was seen in the pallidum (Figure 5C), including both the external and internal segments. Consistent with the topographic nature of the striato-pallidal projection (Cowan and Powell, 1966; Haber et al., 1990; Heilbronner et al., 2018), these terminal fields were in the ventral and lateral portions of the dorsal GPe and GPi, a very different portion of the pallidum than observed in Case 3. There was also substantial anterograde labeling in substantia nigra, likely involving both the pars compacta and pars reticulata (Figure 5D).

Case 5: cStr—We did not observe substantial anterograde labeling in this case, but as noted above, relatively little of the virus was deposited into the gray matter where it could be taken up by cell bodies.

DISCUSSION

Since its development, rAAV2-retro -- a recently engineered recombinant AAV (Tervo et al., 2016)-- has been widely used to characterize the anatomy and function of a range of circuits in rodents (Balmer and Trussell, 2019; Birdsong et al., 2019; Chen et al., 2020; Conner et al., 2019; Hashimoto et al., 2018; Jackson et al., 2018; Lilley et al., 2019; Miller et al., 2019; Ren et al., 2018; Sun et al., 2019a; Wang et al., 2018; Zheng et al., 2020). We aimed to anatomically characterize rAAV2-retro's transgene expression in rhesus macaques to assess its potential for use in monkey chemo- and optogenetic studies. Our results suggest that rAAV2-retro's highly efficient retrograde axonal transport is conserved across species. Thus, rAAV2-retro is a promising candidate for reliable, robust expression of actuator proteins in target neuronal populations in rhesus macaques. Notably, however, we identified a few regions with afferent projections to our injection sites that were not retrogradely labeled by rAAV2-retro. In addition, rAAV2-retro robustly labeled terminal fields in many areas that receive direct projections from the injected structures. Both of these factors have the potential to dramatically impact which circuits are affected by manipulation techniques. Therefore, our results highlight the importance of anatomically characterizing rAAV2-retro in target circuits prior to employing it in physiological or behavioral experiments in NHPs.

rAAV2-retro produces robust, but selective, retrograde labeling

Micro-infusions of rAAV2-retro in rhesus macaque striatal and oculomotor structures produced local infection at injection sites and extensive retrograde labeling of cell bodies in

brain areas with direct projections to the injection site. Efficacy of retrograde transport is difficult to quantify, as determining precisely how many cells in a given brain area project to the injected region within a structure is challenging. In addition, the threshold for the degree of retrograde transport required to elicit a behavioral change via opto- or chemogenetics is unknown, and likely varies by structure and circuit. Thus, in our study, we aimed to provide a qualitative, rather than quantitative, picture of the degree of labeling achieved with rAAV2-retro to serve as a basis for more sophisticated studies of the relationship between degree of labeling and physiological or behavioral effects in specific circuits. Future quantitative analyses of these relationships are required.

Our findings reproduced the well-established anatomical connectivity of the unique NHP cortico-striatal and oculomotor circuits. The retrograde labeling produced by rAAV2-retro was, in many areas, comparable in both pattern and density to that produced by conventional retrograde tract-tracers (Haber, 2016; Haber et al., 1995; Leichnetz and Goldberg, 1988; May, 2006). Moreover, our results corroborate those described by Weiss et al (2020) (with some exceptions, discussed below), who injected rAAV2-retro into the striatum of rhesus macaques (Weiss et al., 2020). They too observed extensive retrograde labeling in many regions. They compared rAAV2-retro to AAV2 and found that, in contrast to rAAV2-retro, AAV2's labeling was largely confined to the injected structures. This confirms rAAV2-retro's superior retrograde axonal transport in macaques and supports our claim that it is a promising tool for dissecting neural circuits in NHPs.

Although we observed retrograde labeling in most expected areas following rAAV2-retro injection, we, intriguingly, identified at least one brain area in every case (1–5) that appeared devoid of retrograde labeling, despite having well-established afferent projections to the rAAV2-retro injection site. For example, while classical tracer studies show strong projections from substantia nigra pars compacta to striatum (Carpenter and Peter, 1972; Haber et al., 2000) and substantia nigra pars reticulata to SC (Jayaraman et al., 1977; Beckstead and Frankfurter, 1982; May, 2006), we found no labeled cells in any subdivision of the substantia nigra following rAAV2-retro injection in striatum or SC (Cases 1; 3–5). Similarly, while classical tracer studies show strong projections from mediodorsal thalamus to FEF (Leichnetz and Goldberg, 1988), we found no labeled cells in mediodorsal thalamus following rAAV2-retro injection in FEF (Case 2). rAAV2-retro exhibited this pattern of cellular tropism irrespective of animal survival time (from ~1–8 months). Viral tropism is complex and multifactorial, but generally falls under one of two categories: receptor-dependent (i.e. viral uptake restricted by the absence of necessary cell-surface receptor(s)) or receptor-independent (i.e. viral replication restricted post-cell entry) (Nomaguchi et al., 2012). Whether rAAV2-retro's cellular tropism is receptor-dependent, receptor independent, or a combination of the two, remains unknown.

Pillay and colleagues (2016) recently identified a receptor – AAV receptor (AAVR) – that is essential for infection by all AAV serotypes (Pillay et al., 2016). It remains unknown whether rAAV2-retro uses AAVR to enter cells or whether it employs a novel cell entry mechanism. Regardless, the absence of rAAV2-retro's cell surface receptor is unlikely to explain its selective retrograde labeling in our study – at least in our striatal injections. In contrast to our results, Weiss et al (2020) reported transgene expression in substantia nigra

pars compacta following injection of a different rAAV2-retro construct into the striatum of rhesus macaques (Weiss et al., 2020). Their results indicate that the terminals of macaque substantia nigra pars compacta neurons in striatum very likely express the necessary receptor(s) for rAAV2-retro cell entry. We suspect, therefore, that intracellular factors, rather than restricted cell entry, are responsible for rAAV2-retro's selective expression pattern in our hands. Moreover, Tervo et al (2016) reported a few classes of projection neurons in rodents that seemed resistant to retrograde labeling by rAAV2-retro. However, in some of these projections (e.g. corticothalamic and corticobulbar projections), rAAV2-retro delivery of Cre recombinase resulted in robust Cre-dependent transgene expression. Because only small amounts of Cre recombinase are necessary to drive expression, this finding suggests that rAAV2-retro is capable of delivering transgene to these neurons, but transgenic protein expression is weak. This, again, supports our hypothesis that rAAV2-retro's selective labeling is not a function of cell-surface receptor availability; rather, it is a function of intracellular factors. We suspect that similar experiments in macaques would reveal the same result, but additional work is needed for confirmation. Thus, optical or ligand-mediated manipulation of areas in which we expected, but did not observe, retrograde labeling may elicit neural responses via small amounts of transgenic actuators that were undetectable using our visualization methods. Physiological experiments are needed to test this.

Several research groups have reported discrepancies in transport properties of AAVs when the same serotype is used (Aschauer et al., 2013; Burger et al., 2004a; Cearley et al., 2008; Kaspar et al., 2002; Masamizu et al., 2011; Salegio et al., 2013; Zingg et al., 2017). Promoter choice is likely to play a role in these discrepancies. For example, we used human synapsin (hSyn) and Calcium/calmodulin-dependent kinase II alpha subunit (CaMKII) promoters in our striatal injections. Weiss et al (2020) used cytomegalovirus (CMV) and CMV early enhancer/chicken β actin (CAG) promoters. Studies in NHPs have shown that cellular transduction patterns vary with viral serotype, promoter, and brain area injected (Benson et al., 1991; Gerits et al., 2015; Lerchner et al., 2014; Watakabe et al., 2015; Wu et al., 2017; Yaguchi et al., 2013). Future experiments comparing rAAV2-retro labeling patterns with different promoters, both within and across multiple brain areas, are needed.

Galvan and colleagues (2019) found that large fluorescent tags, such as mCherry, on viral constructs encoding certain DREADDs, interfere with plasma membrane trafficking of those DREADDs in NHPs (Galvan et al., 2019). Replacing mCherry with a much smaller tag, haemagglutinin (HA), improved membrane trafficking (Galvan et al., 2019). In addition, Yazdan-Shahmorad and colleagues (2018) reported lower transgenic protein expression levels in monkeys injected with viral constructs encoding an opsin fused to mCherry compared to ones encoding an opsin fused to YFP (Yazdan-Shahmorad et al., 2018). Our study did not directly test the effects of protein tag choice on rAAV2-retro's retrograde labeling. The viral vector used in one of our striatal injections (Case 4) carried an HA tag, in contrast to the mCherry tag on the viral vectors used in the other two striatal injections (Cases 3&5). Nevertheless, none of the striatal injections, which share common anatomical connections, produced nigral labeling. It is important to note, however, that the promoter on these constructs also differed (hSyn in Case 4 versus CaMKII in Cases 3&5). Viruses encoding different tags were not tested in FEF and SC. Therefore, no concrete conclusions can be drawn about tag choice from our results, and our visualization methods do not allow

for precise cellular or subcellular localization of the actuator proteins. Future experiments comparing rAAV2-retro labeling patterns with different reporter tags are needed.

Finally, we considered the possibility that animal survival times may affect rAAV2-retro transduction patterns but concluded that this is unlikely. We examined a wide range of survival times in our study (~1–8 months) and found that rAAV2-retro consistently produced selective retrograde labeling. We did not, however, examine the effects of varying injection volume and titer or using different injection methods, such as convection enhanced delivery (CED). CED has been reported to improve transduction levels in NHPs. It creates a pressure gradient that increases the spread of the viral solution through the parenchyma of the brain rather than depending solely on the properties of diffusion like the conventional micro-injection technique used in our study. CED allows for faster injection rates, and results in widespread and uniform transduction (Bankiewicz et al., 2000; Cunningham et al., 2008; Johnston et al., 2009; Kells et al., 2009; Khateeb et al., 2019; Yazdan-Shahmorad et al., 2018, 2016). However, our use of multiple micro-injections in each structure likely produced a similar spread to that achieved with CED, as we saw extensive retrograde transport that indicates that this variable does not account for the selectivity of the retrograde transport. Additionally, micro-injections allow for targeted focal expression when necessary.

Overall, although false negatives were observed in our study, we have identified viral constructs that are effective for delivering transgene to key projections such as the cortico-striatal projection and the FEF-SC projection.

rAAV2-retro labels axon terminals in rhesus macaque cortico-basal ganglia and oculomotor circuits

In almost every case (1–4) we observed extensive labeling of axon terminals in many brain areas. For example, we found labeled terminal fields in mediodorsal thalamus and throughout the brainstem following rAAV2-retro injection in SC and FEF (Cases 1&2). Similarly, we found labeled terminal fields in globus pallidus and substantia nigra following rAAV2-retro injection in striatum (Cases 3&4). The patterns and density of labeled terminal fields produced by our rAAV2-retro injections closely replicate those produced by conventional anterograde tracers injected in the same structures (Basso and May, 2017; Haber et al., 1990; Harting 1977; Harting et al., 1980; Heilbronner et al., 2018; Huerta et al., 1986; Stanton et al., 1988A&B). There are at least two possible mechanisms for the axon terminal labeling in our cases. rAAV2-retro may infect cell bodies at the injection site, much like other AAV serotypes, and fill the axons and axon terminals of infected cells with exogenous protein. Alternatively, it may infect terminals of short axon collaterals local to the injection site, be retrogradely transported to cell bodies, then fill the long projection axons of those cell bodies with exogenous protein. For example, striatal medium spiny neurons have extensive short axon collaterals near the soma, as well as long-distance projections to the pallidum and substantia nigra (pars reticulata and pars compacta) (Preston et al., 1980). Similarly, the crossed output cells of the SC intermediate gray layer have local axon collaterals (Moschovakis et al., 1988).

Regardless of mechanism, it is important to note the functional implications of such labeled terminal fields on opto- and chemogenetic studies in NHPs. For example, in our study,

optical stimulation or intracranial injection of the DREADD ligand in mediodorsal thalamus following rAAV2-retro injection in FEF would result in manipulation of FEF-mediodorsal thalamus projections, but not mediodorsal thalamus-FEF projections. This is due to the fact that axon terminals were labeled in mediodorsal thalamus, but cell bodies, unexpectedly, were not. Taken together, the findings of selective retrograde labeling and terminal field labeling produced by rAAV2-retro in our study highlight the importance of anatomically characterizing transgene expression by viruses before employing them in NHP chemo- and optogenetic experiments. Bypassing anatomical characterization may result in unknowingly exciting or inhibiting an unintended brain circuit during physiological and behavioral experiments. Rodent studies employing rAAV2-retro have not frequently reported terminal field labeling. However, implications of axon terminal labeling in rodent opto- and chemogenetic studies are not as severe given that axon terminal labeling is easily mitigated by using transgenic technology and Cre-dependent expression, two very common methods in rodent studies. However, in NHPs, such technologies are difficult, so anatomical characterization of viral vectors in these animal models is critical.

rAAV2-retro safety

Many retrogradely transported viruses such as rabies virus, herpes simplex virus, canine adenovirus type 2, and some pseudotyped lentiviruses can be neurotoxic (Bohlen et al., 2019; Tanabe et al., 2019; Callaway and Luo, 2015; Ginger et al., 2013; Marconi et al., 2008; Schnell et al., 2010). In the current study, rAAV2-retro did not cause any obvious behavioral changes in the injected animals, and our histological processing did not reveal any visible signs of gliosis, suggesting that rAAV2-retro is relatively safe. Glial marker immunostaining following rAAV2-retro injections in rodents (Sun et al., 2019a) and rhesus macaques (Weiss et al, 2020) showed that rAAV2-retro does not produce significant toxic effects. In addition, after an 8-month survival period (Case 1), we still observed robust transgene expression, indicating that long periods of transgene accumulation did not elicit an immune response that affected expression levels.

Future directions

In this study, we anatomically characterized rAAV2-retro expression in rhesus macaques. Our results suggest that it is a promising vector for delivery of exogenous genes encoding actuator proteins, such as opsins and chemogenetic receptors, in rhesus macaques. Future experiments will be aimed at validating the functional efficacy of protein actuators delivered by rAAV2-retro in rhesus macaque opto- and chemogenetic studies. In parallel, additional experiments are needed to identify optimal rAAV2-retro injection parameters for producing maximal spread and transgene expression, without initiating an immune response. More work is also needed to elucidate rAAV2-retro's cell entry mechanism and determine the effect of promoter choice and reporter tag on patterns of transgenic protein expression. Future experiments could also explore using rAAV2-retro in combination with other retrograde viruses to define the complete connectivity of circuits, since other retrograde viruses have also been reported to exhibit selective retrograde labeling (Sun et al., 2019a). Alternatively, AAV variants with tailored tropism (Davidsson et al, 2019) could be used to label specific projections in which rAAV2-retro's retrograde axonal transport is inefficient. For example, Davidsson et al (2019) developed an AAV variant that is retrogradely

transported in dopaminergic neurons, such as the nigrostriatal projection neurons that rAAV2-retro failed to label in our hands. NeuRet, a recently developed pseudotyped lentiviral vector, is another promising candidate that robustly labels nigrostriatal projections and is minimally immunogenic (Kato et al., 2011b; Tanabe et al., 2019). Another future direction to explore is using rAAV2-retro in intersectional methods. Its robust retrograde transport makes it a promising virus to employ in such techniques (Conner et al., 2019). While some NHP studies have successfully achieved Cre-driven transgene expression via intersectional methods (O'Shea et al., 2018; Stauffer et al., 2016; Oguchi et al., 2015), such methods remain challenging and need optimization. Future experiments could also explore injecting rAAV2-retro using convection enhanced delivery, which has been reported to improve transduction levels in monkeys (Bankiewicz et al., 2000; Cunningham et al., 2008; Johnston et al., 2009; Kells et al., 2009; Khateeb et al., 2019; Yazdan-Shahmorad et al., 2018, 2016). Lastly, rAAV2-retro has already been used in rhesus macaques to deliver transgenes for creating new disease models (Weiss et al., 2020). Therefore, rAAV2-retro shows great promise for use in gene therapies for the treatment of a wide range of neurological diseases and neuropsychiatric disorders, but more work is needed to explore rAAV2-retro's potential in the clinical realm.

ACKNOWLEDGMENTS

We would like to acknowledge data collection assistance from Tanya Casta, Reed Evers, Mark Grier, Mahtahn Jenkins, Megan Monko, Kelsey Person, and Zane Crabtree and the histological assistance of Jinrong Wei. We would like to acknowledge funding from a UMN Medical Discovery Team on Addiction Pilot Grant (SRH), NIH T32DA007234 (AKC), the Hartwell Biomedical Research Fellowship (MOB), the Duke Institute for Brain Sciences Germinator Award (MOB and MAS), and the National Institutes of Health (NEI R21 EY030278 to MAS), as well as NIH grant EY014263 to PJM and EY013692 to MAB. All viral vectors used at the University of Minnesota were generated by the University of Minnesota Viral Vector and Cloning Core (Minneapolis, MN).

REFERENCES

Acker L, Pino EN, Boyden ES, Desimone R, 2016 FEF inactivation with improved optogenetic methods. Proc. Natl. Acad. Sci. U. S. A 113, E7297–E7306. 10.1073/pnas.1610784113 [PubMed: 27807140]

Afraz A, Boyden ES, DiCarlo JJ, 2015 Optogenetic and pharmacological suppression of spatial clusters of face neurons reveal their causal role in face gender discrimination. Proc. Natl. Acad. Sci. U. S. A 112, 6730–6735. 10.1073/pnas.1423328112 [PubMed: 25953336]

Aponte-Ubillus JJ, Barajas D, Peltier J, Bardliving C, Shamlou P, Gold D, 2018 Molecular design for recombinant adeno-associated virus (rAAV) vector production. Appl. Microbiol. Biotechnol 102, 1045–1054. 10.1007/s00253-017-8670-1 [PubMed: 29204900]

Arikuni T, Kubota K, 1985 Claustral and amygdaloid afferents to the head of the caudate nucleus in macaque monkeys. Neurosci. Res 2, 239–254. 10.1016/0168-0102(85)90003-3 [PubMed: 4022459]

Aschauer DF, Kreuz S, Rumpel S, 2013 Analysis of Transduction Efficiency, Tropism and Axonal Transport of AAV Serotypes 1, 2, 5, 6, 8 and 9 in the Mouse Brain. PLoS One 8, 1–16. 10.1371/journal.pone.0076310

Balmer TS, Trussell LO, 2019 Selective targeting of unipolar brush cell subtypes by cerebellar mossy fibers. 10.7554/eLife.44964.001

Bankiewicz KS, Eberling JL, Kohutnicka M, Jagust W, Pivirotto P, Bringas J, Cunningham J, Budinger TF, Harvey-White J, 2000 Convection-Enhanced Delivery of AAV Vector in Parkinsonian Monkeys; In Vivo Detection of Gene Expression and Restoration of Dopaminergic Function Using Pro-drug Approach 10.1006/exnr.2000.7408

Basso MA, May PJ. 2017 Circuits for action and cognition: A view from the superior colliculus. Annu Rev Vis Sci. 3:197–226. doi: 10.1146/annurev-vision-102016-061234. [PubMed: 28617660]

Beckstead RM, Frankfurter A. 1982 The distribution and some morphological features of substantia nigra neurons that project to the thalamus, superior colliculus and pedunculopontine nucleus in the monkey. Neuroscience. 7:2377–88. [PubMed: 7177379]

Benson DL, Isackson PJ, Hendry SHC, Jones EG, 1991 Differential gene expression for glutamic acid decarboxylase and type II calcium-calmodulin-dependent protein kinase in basal ganglia, thalamus, and hypothalamus of the monkey. J. Neurosci 11, 1540–1564. 10.1523/jneurosci.11-06-01540.1991 [PubMed: 1646294]

Birdsong WT, Jongbloets BC, Engeln KA, Wang D, gory Scherrer G, Mao T, 2019 Synapse-specific opioid modulation of thalamo-cortico-striatal circuits. 10.7554/eLife.45146.001

Bohlen MO, El-Nahal HG, Sommer MA, 2019 Transduction of Craniofacial Motoneurons Following Intramuscular Injections of Canine Adenovirus Type-2 (CAV-2) in Rhesus Macaques. Front. Neuroanat 13 10.3389/fnana.2019.00084 [PubMed: 30837847]

Büeler H, 1999 Adeno-associated viral vectors for gene transfer and gene therapy. Biol. Chem 380, 613–622. 10.1515/BC.1999.078 [PubMed: 10430026]

Burger C, Gorbatyuk OS, Velardo MJ, Peden CS, Williams P, Zolotukhin S, Reier PJ, Mandel RJ, Muzyczka N, 2004a Recombinant AAV viral vectors pseudotyped with viral capsids from serotypes 1, 2, and 5 display differential efficiency and cell tropism after delivery to different regions of the central nervous system. Mol. Ther 10, 302–317. 10.1016/j.ymthe.2004.05.024 [PubMed: 15294177]

Callaway EM, Luo L, 2015 Monosynaptic circuit tracing with glycoprotein-deleted rabies viruses. J. Neurosci 35, 8979–8985. 10.1523/JNEUROSCI.0409-15.2015 [PubMed: 26085623]

Carpenter MB, Peter P, 1972 Nigrostriatal and nigrothalamic fibers in the rhesus monkey. J. Comp. Neurol 144, 93–115. 10.1002/cne.901440105 [PubMed: 4623850]

Castle MJ, Gershenson ZT, Giles AR, Holzbaur ELF, Wolfe JH, 2014 Adeno-associated virus serotypes 1, 8, and 9 share conserved mechanisms for anterograde and retrograde axonal transport. Hum. Gene Ther 25, 705–720. 10.1089/hum.2013.189 [PubMed: 24694006]

Cavanaugh J, Monosov IE, Mcalonan K, Berman R, Smith MK, Cao V, Wang KH, Boyden ES, Wurtz RH, 2012 Optogenetic Inactivation Modifies Monkey Visuomotor Behavior. Neuron 76, 901–907. 10.1016/j.neuron.2012.10.016 [PubMed: 23217739]

Cearley CN, Vandenberghe LH, Parente MK, Carnish ER, Wilson JM, Wolfe JH, 2008 Expanded repertoire of AAV vector serotypes mediate unique patterns of transduction in mouse brain. Mol. Ther 16, 1710–1718. 10.1038/mt.2008.166 [PubMed: 18714307]

Chen Z, Fan G, Li A, Yuan J, Xu T, 2020 rAAV2-Retro Enables Extensive and High-Efficient Transduction of Lower Motor Neurons following Intramuscular Injection. Mol. Ther. - Methods Clin. Dev 17, 21–33. 10.1016/j.omtm.2019.11.006 [PubMed: 31890738]

Choi VW, McCarty DM, Samulski RJ, 2006 Host Cell DNA Repair Pathways in Adeno-Associated Viral Genome Processing. J. Virol 80, 10346–10356. 10.1128/jvi.00841-06 [PubMed: 17041215]

Conner JM, Bain GL, Dulin JN, 2019 Intraspinal and intracortical delivery of AAV vectors for intersectional circuit tracing in non-transgenic species, in: Methods in Molecular Biology. Humana Press Inc, pp. 165–176. 10.1007/978-1-4939-9139-6_9

Cowan WM, Powell TP, 1966 Strio-pallidal projection in the monkey. J. Neurol. Neurosurg. Psychiatry 29, 426–439. 10.1136/jnnp.29.5.426 [PubMed: 4959016]

Cunningham J, Pivirotto P, Bringas J, Suzuki B, Vijay S, Sanftner L, Kitamura M, Chan C, Bankiewicz KS, 2008 Biodistribution of adeno-associated vrus type-2 in nonhuman primates after convection-enhanced delivery to brain. Mol. Ther 16, 1267–1275. 10.1038/mt.2008.111 [PubMed: 18523450]

Dai J, Brooks DI, Sheinberg DL, 2014 Optogenetic and electrical microstimulation systematically bias visuospatial choice in primates. Curr. Biol 24, 63–69. 10.1016/j.cub.2013.11.011 [PubMed: 24332543]

Davidsson M, Wang G, Aldrin-Kirk P, Cardoso T, Nolbrant S, Hartnor M, Mudannayake J, Parmar M, Björklund T, 2019 A systematic capsid evolution approach performed in vivo for the design of AAV vectors with tailored properties and tropism. Proc. Natl. Acad. Sci. U. S. A 116, 27053–27062. 10.1073/pnas.1910061116

El-Shamayleh Y, Horwitz GD, 2019 Primate optogenetics: Progress and prognosis, in: Proceedings of the National Academy of Sciences of the United States of America. National Academy of Sciences, pp. 26195–26203. 10.1073/pnas.1902284116

El-Shamayleh Y, Kojima Y, Soetedjo R, Horwitz GD, 2017 Selective Optogenetic Control of Purkinje Cells in Monkey Cerebellum. Neuron 95, 51-62.e4. 10.1016/j.neuron.2017.06.002 [PubMed: 28648497]

El-Shamayleh Y, Ni AM, Gregory X, Horwitz D, 2016 Strategies for targeting primate neural circuits with viral vectors. J Neurophysiol 116, 122–134. 10.1152/jn.00087.2016 [PubMed: 27052579]

Ferry AT, Öngür D, An X, Price JL, 2000 Prefrontal cortical projections to the striatum in macaque monkeys: Evidence for an organization related to prefrontal networks. J. Comp. Neurol 425, 447–470. 10.1002/1096-9861(20000925)425:3<447::AID-CNE9>3.0.CO;2-V [PubMed: 10972944]

Fetsch CR, Odean NN, Jeurissen D, El-Shamayleh Y, Horwitz GD, Shadlen MN, 2018 Focal optogenetic suppression in macaque area MT biases direction discrimination and decision confidence, but only transiently. Elife 7 10.7554/eLife.36523

Fries W, 1984 Cortical projections to the superior colliculus in the macaque monkey: A retrograde study using horseradish peroxidase. J. Comp. Neurol 230, 55–76. 10.1002/cne.902300106 [PubMed: 6096414]

Galvan A, Caiola MJ, Albaugh DL, 2018 Advances in optogenetic and chemogenetic methods to study brain circuits in non-human primates. J. Neural Transm 10.1007/s00702-017-1697-8

Galvan A, Hu X, Smith Y, Wichmann T, 2016 Effects of optogenetic activation of corticothalamic terminals in the motor thalamus of awake monkeys. J. Neurosci 36, 3519–3530. 10.1523/JNEUROSCI.4363-15.2016 [PubMed: 27013680]

Galvan A, Raper J, Hu X, Paré J-F, Bonaventura J, Richie CT, Michaelides M, L Mueller SA, Roseboom PH, Oler JA, Hall RA, Smith Y, Adriana Galvan C, 2019 Ultrastructural localization of DREADDs in monkeys. Eur J Neurosci 50, 2801–2813. 10.1111/ejn.14429 [PubMed: 31063250]

Galvan A, Stauffer WR, Acker L, El-Shamayleh Y, Inoue KI, Ohayon S, Schmid MC, 2017 Nonhuman primate optogenetics: Recent advances and future directions. J. Neurosci 10.1523/JNEUROSCI.1839-17.2017

Gerits A, Vancraeyenest P, Vreysen S, Laramée M-E, Michiels A, Gijsbers R, Van den Haute C, Moons L, Debyser Z, Baekelandt V, Arckens L, Vanduffel W, 2015 Serotype-dependent transduction efficiencies of recombinant adeno-associated viral vectors in monkey neocortex. Neurophotonics 2, 031209 10.1117/1.nph.2.3.031209 [PubMed: 26839901]

Ginger M, Haberl M, Conzelmann KK, Schwarz MK, Frick A, 2013 Revealing the secrets of neuronal circuits with recombinant rabies virus technology. Front. Neural Circuits 10.3389/fncir.2013.00002

Grayson DS, Bliss-Moreau E, Machado CJ, Bennett J, Shen K, Grant KA, Fair DA, Amaral DG, 2016 The Rhesus Monkey Connectome Predicts Disrupted Functional Networks Resulting from Pharmacogenetic Inactivation of the Amygdala. Neuron 91, 453–466. 10.1016/j.neuron.2016.06.005 [PubMed: 27477019]

Grimaldi P, Cho SH, Lau H, Basso MA, 2018 Superior colliculus signals decisions rather than confidence: analysis of single neurons. J. Neurophysiol 120, 2614–2629. 10.1152/jn.00152.2018 [PubMed: 30183470]

Haber SN, 2016 Corticostriatal circuitry. Dialogues Clin Neurosci. 18(1): 7–21. [PubMed: 27069376]

Haber SN, Fudge JL, Mcfarland NR, 2000 Striatonigrostriatal Pathways in Primates Form an Ascending Spiral from the Shell to the Dorsolateral Striatum.

Haber SN, Kim KS, Mailly P, Calzavara R, 2006 Reward-related cortical inputs define a large striatal region in primates that interface with associative cortical connections, providing a substrate for incentive-based learning. J. Neurosci 26, 8368–8376. 10.1523/JNEUROSCI.0271-06.2006 [PubMed: 16899732]

Haber SN, Kunishio K, Mizobuchi M, Lynd-Balta E, 1995 The orbital and medial prefrontal circuit through the primate basal ganglia. J. Neurosci 15, 4851–4867. 10.1523/jneurosci.15-07-04851.1995 [PubMed: 7623116]

Haber SN, Lynd E, Klein C, Groenewegen AHJ, 1990 Topographic Organization of the Ventral Striatal Efferent Projections i n the Rhesus Monkey : An Anterograde Tracing Study 298.

Hadaczek P, Stanek L, Ciesielska A, Sudhakar V, Samaranch L, Pivirotto P, Bringas J, O'Riordan C, Mastis B, San Sebastian W, Forsayeth J, Cheng SH, Bankiewicz KS, Shihabuddin LS, 2016 Widespread AAV1- and AAV2-mediated transgene expression in the nonhuman primate brain: implications for Huntington's disease. Mol. Ther. - Methods Clin. Dev 3, 16037 10.1038/mtm.2016.37 [PubMed: 27408903]

Harting JK., 1977 Descending pathways from the superior collicullus: an autoradiographic analysis in the rhesus monkey (Macaca mulatta). J Comp Neurol 173(3):583–612. [PubMed: 404340]

Harting JK, Huerta MF, Frankfurter AJ, Strominger NL, Royce GJ. 1980 Ascending pathways from the monkey superior colliculus: an autoradiographic analysis. J Comp Neurol 192(4):853–82. [PubMed: 7419758]

Hashimoto M, Yamanaka A, Kato S, Tanifuji M, Kobayashi K, Yaginuma H, 2018 Anatomical evidence for a direct projection from purkinje cells in the mouse cerebellar vermis to medial parabrachial nucleus. Front. Neural Circuits 12 10.3389/fncir.2018.00006

Heilbronner SR, Meyer MAA, Choi EY, Haber SN, 2018 How do cortico-striatal projections impact on downstream pallidal circuitry? Brain Struct. Funct 223, 2809–2821. 10.1007/s00429-018-1662-9 [PubMed: 29654360]

Hong J, Heo W. Do, 2020 Optogenetic Modulation of TrkB Signaling in the Mouse Brain. J. Mol. Biol 432, 815–827. 10.1016/j.jmb.2020.01.010 [PubMed: 31962123]

Huerta MF, Krubitzer LA, Kaas JH. 1986 Frontal eye field as defined by intracortical microstimulation in squirrel monkeys, owl monkeys, and macaque monkeys: I. Subcortical connections. J Comp Neurol. 253(4):415–39. [PubMed: 3793998]

Inoue K, Koketsu D, Kato S, Kobayashi K, Nambu A, Takada M, 2012 Immunotoxin-Mediated Tract Targeting in the Primate Brain: Selective Elimination of the Cortico-Subthalamic "Hyperdirect" Pathway. PLoS One 7, e39149 10.1371/journal.pone.0039149 [PubMed: 22761729]

Inoue KI, Takada M, Matsumoto M, 2015 Neuronal and behavioural modulations by pathway-selective optogenetic stimulation of the primate oculomotor system. Nat. Commun 6 10.1038/ncomms9378

Jayaraman A, Batton RR 3rd, Carpenter MB. 1977 Nigrotectal projections in the monkey: an autoradiographic study. Brain Res. 135:147–52 [PubMed: 410480]

Jackson J, Karnani MM, Zemelman BV, Burdakov D, Lee AK, 2018 Inhibitory Control of Prefrontal Cortex by the Claustrum. Neuron 99, 1029–1039.e4. 10.1016/j.neuron.2018.07.031 [PubMed: 30122374]

Jin Bak I, Markham CH, Cook ML, Stevens JG, 1977 Intraaxonal transport of Herpes simplex virus in the rat central nervous system. Brain Res. 136, 415–429. 10.1016/0006-8993(77)90067-1 [PubMed: 72587]

Johnston LC, Eberling J, Pivirotto P, Hadaczek P, Federoff HJ, Forsayeth J, Bankiewicz KS, 2009 Clinically relevant effects of convection-enhanced delivery of AAV2-GDNF on the dopaminergic nigrostriatal pathway in aged rhesus monkeys. Hum. Gene Ther 20, 497–510. 10.1089/hum.2008.137 [PubMed: 19203243]

Ju N, Jiang R, Macknik SL, Martinez-Conde S, Tang S, 2018 Long-term all-optical interrogation of cortical neurons in awake-behaving nonhuman primates. PLOS Biol. 16, e2005839 10.1371/journal.pbio.2005839 [PubMed: 30089111]

Kaspar BK, Erickson D, Schaffer D, Hinh L, Gage FH, Peterson DA, 2002 Targeted retrograde gene delivery for neuronal protection. Mol. Ther 5, 50–56. 10.1006/mthe.2001.0520 [PubMed: 11786045]

Kato S, Kobayashi Kenta, Inoue K-I, Kuramochi M, Okada T, Yaginuma H, Morimoto K, Shimada T, Takada M, Kobayashi Kazuto, 2011a A Lentiviral Strategy for Highly Efficient Retrograde Gene Transfer by Pseudotyping with Fusion Envelope Glycoprotein 10.1089/hum.2009.179

Kato S, Kuramochi M, Takasumi K, Kobayashi Kenta, Inoue K-I, Takahara D, Hitoshi S, Ikenaka K, Shimada T, Takada M, Kobayashi Kazuto, 2011b Neuron-Specific Gene Transfer Through Retrograde Transport of Lentiviral Vector Pseudotyped with a Novel Type of Fusion Envelope Glycoprotein 10.1089/hum.2011.111

Kells AP, Hadaczek P, Yin D, Bringas J, Varenika V, Forsayeth J, Bankiewicz KS, 2009 Efficient gene therapy-based method for the delivery of therapeutics to primate cortex.

Khateeb K, Griggs DJ, Sabes PN, Yazdan-Shahmorad A, 2019 Convection enhanced delivery of optogenetic adeno-associated viral vector to the cortex of rhesus macaque under guidance of online MRI images. J. Vis. Exp 2019, e59232 10.3791/59232

Kinoshita M, Kato R, Isa K, Kobayashi Kenta, Kobayashi Kazuto, Onoe H, Isa T, 2019 Dissecting the circuit for blindsight to reveal the critical role of pulvinar and superior colliculus. Nat. Commun 10, 1–10. 10.1038/s41467-018-08058-0 [PubMed: 30602773]

Kinoshita M, Matsui R, Kato S, Hasegawa T, Kasahara H, Isa K, Watakabe A, Yamamori T, Nishimura Y, Alstermark B, Watanabe D, Kobayashi K, Isa T, 2012 Genetic dissection of the circuit for hand dexterity in primates. Nature 487, 235–238. 10.1038/nature11206 [PubMed: 22722837]

Kita H, Tokuno H, Nambu A, 1999 Monkey globus pallidus external segment neurons projecting to the neostriatum. Neuroreport 10, 1467–1472. 10.1097/00001756-199905140-00014 [PubMed: 10380964]

Klein C, Evrard HCC, Shapcott KAA, Haverkamp S, Logothetis NKK, Schmid MCC, 2016 Cell-Targeted Optogenetics and Electrical Microstimulation Reveal the Primate Koniocellular Projection to Supra-granular Visual Cortex. Neuron 90, 143–151. 10.1016/j.neuron.2016.02.036 [PubMed: 27021172]

Künzle H, 1977 Projections from the primary somatosensory cortex to basal ganglia and thalamus in the monkey. Exp. Brain Res 30, 481–492. 10.1007/BF00237639 [PubMed: 413731]

Lee WH, Lisanby SH, Laine AF, Peterchev AV, 2017 Minimum Electric Field Exposure for Seizure Induction with Electroconvulsive Therapy and Magnetic Seizure Therapy. Neuropsychopharmacology 42, 1192–1200. 10.1038/npp.2016.276 [PubMed: 27934961]

Lee WH, Lisanby SH, Laine AF, Peterchev AV, 2015 Electric Field Model of Transcranial Electric Stimulation in Nonhuman Primates: Correspondence to Individual Motor Threshold. IEEE Trans. Biomed. Eng 62, 2095–2105. 10.1109/TBME.2015.2425406 [PubMed: 25910001]

Leichnetz GR, 1982 Connections between the frontal eye field and pretectum in the monkey: An anterograde/retrograde study using HRP GEL and TMB neurohistochemistry. J. Comp. Neurol 207, 394–402. 10.1002/cne.902070410 [PubMed: 7119150]

Leichnetz GR, Goldberg ME, 1988 Higher centers concerned with eye movement and visual attention: cerebral cortex and thalamus. Rev. Oculomot. Res 2, 365–429. [PubMed: 3153653]

Leichnetz GR, Spencer RF, Hardy SGP, Astruc J, 1981 The prefrontal corticotectal projection in the monkey; An anterograde and retrograde horseradish peroxidase study. Neuroscience 6, 1023–1041. 10.1016/0306-4522(81)90068-3 [PubMed: 6168970]

Lerchner W, Corgiat B, Der Minassian V, Saunders RC, Richmond BJ, 2014 Injection parameters and virus dependent choice of promoters to improve neuron targeting in the nonhuman primate brain. Gene Ther. 21, 233–241. 10.1038/gt.2013.75 [PubMed: 24401836]

Lilley BN, Sabbah S, Hunyara JL, Gribble KD, Al-Khindi T, Xiong J, Wu Z, Berson DM, Kolodkin AL, 2019 Genetic access to neurons in the accessory optic system reveals a role for Sema6A in midbrain circuitry mediating motion perception. J. Comp. Neurol 527, 282–296. 10.1002/cne.24507 [PubMed: 30076594]

Li X, Yamawaki N, Barrett JM, Körding KP, Shepherd GMG, 2018 Scaling of Optogenetically Evoked Signaling in a Higher-Order Corticocortical Pathway in the Anesthetized Mouse. Front. Syst. Neurosci 12, 16 10.3389/fnsys.2018.00016 [PubMed: 29867381]

Lu Y, Truccolo W, Wagner FB, Vargas-Irwin CE, Ozden I, Zimmermann JB, May T, Agha NS, Wang J, Nurmikko AV, 2015 Optogenetically induced spatiotemporal gamma oscillations and neuronal spiking activity in primate motor cortex. J. Neurophysiol 113, 3574–3587. 10.1152/jn.00792.2014 [PubMed: 25761956]

Maeda K, Inoue K. ichi, Kunimatsu J, Takada M, Hikosaka O, 2020 Primate Amygdalo-Nigral Pathway for Boosting Oculomotor Action in Motivating Situations. iScience 23, 101194 10.1016/j.isci.2020.101194 [PubMed: 32516719]

Marconi P, Argnani R, Berto E, Epstein AL, Manservigi R, 2008 HSV as a vector in vaccine development and gene therapy. Hum. Vaccin 10.4161/hv.4.2.6212

Masamizu Y, Okada T, Kawasaki K, Ishibashi H, Yuasa S, Takeda S, Hasegawa I, Nakahara K, 2011 Local and retrograde gene transfer into primate neuronal pathways via adeno-associated virus

serotype 8 and 9. Neuroscience 193, 249–258. 10.1016/j.neuroscience.2011.06.080 [PubMed: 21782903]

May PJ, Hartwich-Young R, Nelson J, Sparks DL, Porter JD. 1990 Cerebellotectal pathways in the macaque: implications for collicular generation of saccades. Neuroscience. 36(2):305–24. [PubMed: 2215926]

May PJ, 2006 The mammalian superior colliculus: Laminar structure and connections. Prog. Brain Res 10.1016/S0079-6123(05)51011-2

May T, Ozden I, Brush B, Borton D, Wagner F, Agha N, Sheinberg DL, Nurmikko AV, 2014 Detection of Optogenetic Stimulation in Somatosensory Cortex by Non-Human Primates - Towards Artificial Tactile Sensation. PLoS One 9, e114529 10.1371/journal.pone.0114529 [PubMed: 25541938]

McFarland NR, Lee JS, Hyman BT, McLean PJ, 2009 Comparison of transduction efficiency of recombinant AAV serotypes 1, 2, 5, and 8 in the rat nigrostriatal system. J. Neurochem 109, 838–845. 10.1111/j.1471-4159.2009.06010.x [PubMed: 19250335]

Miller SM, Marcotulli D, Shen A, Zweifel LS, 2019 Divergent medial amygdala projections regulate approach–avoidance conflict behavior. Nat. Neurosci 22, 565–575. 10.1038/s41593-019-0337-z [PubMed: 30804529]

Monahan PE, Samulski RJ, 2000 Adeno-associated virus vectors for gene therapy: More pros than cons? Mol. Med. Today 10.1016/S1357-4310(00)01810-4

Moschovakis AK, Karabelas AB, Highstein SM. 1988 Structure-function relationships in the primate superior colliculus. I. Morphological classification of efferent neurons. J Neurophysiol. 60(1):232–62. [PubMed: 3404219]

Nagai Y, Kikuchi E, Lerchner W, Inoue K-I, Bin J, Eldridge MAG, Kaneko H, Kimura Y, Oh-Nishi A, Hori Y, Kato Y, Hirabayashi T, Fujimoto A, Kumata K, Zhang M-R, Aoki I, Suhara T, Higuchi M, Takada M, Richmond BJ, Minamimoto T, 2016 PET imaging-guided chemogenetic silencing reveals a critical role of primate rostromedial caudate in reward evaluation. 10.1038/ncomms13605

Nakamichi Y, Okubo K, Sato T, Hashimoto M, Tanifuji M, 2019 Optical intrinsic signal imaging with optogenetics reveals functional cortico-cortical connectivity at the columnar level in living macaques. Sci. Rep 9, 1–12. 10.1038/s41598-019-42923-2 [PubMed: 30626917]

Naso MF, Tomkowicz B, Perry WL, Strohl WR, 2017 Adeno-Associated Virus (AAV) as a Vector for Gene Therapy. BioDrugs 31, 317–334. 10.1007/s40259-017-0234-5 [PubMed: 28669112]

Nassi JJ, Cepko CL, Born RT, Beier KT, 2015 Neuroanatomy goes viral! Front. Neuroanat 10.3389/fnana.2015.00080

Nomaguchi M, Fujita M, Miyazaki Y, Adachi A, 2012 Viral tropism. Front. Microbiol 10.3389/fmicb.2012.00281

Nurminen L, Merlin S, Bijanzadeh M, Federer F, Angelucci A, 2018 Top-down feedback controls spatial summation and response amplitude in primate visual cortex. Nat. Commun 9, 1–13. 10.1038/s41467-018-04500-5 [PubMed: 29317637]

Odegaard B, Grimaldi P, Cho SH, Peters MAK, Lau H, Basso MA, 2018 Superior colliculus neuronal ensemble activity signals optimal rather than subjective confidence. Proc. Natl. Acad. Sci. U. S. A 115, E1588–E1597. 10.1073/pnas.1711628115 [PubMed: 29382765]

Oguchi M, Okajima M, Tanaka S, Koizumi M, Kikusui T, Ichihara N, Kato S, Kobayashi K, Sakagami M, 2015 Double Virus Vector Infection to the Prefrontal Network of the Macaque Brain. 10.1371/journal.pone.0132825

Ojala DS, Amara DP, Schaffer DV, 2015 Adeno-associated virus vectors and neurological gene therapy. Neuroscientist 21, 84–98. 10.1177/1073858414521870 [PubMed: 24557878]

O'Shea DJ, Kalanithi P, Ferenczi EA, Hsueh B, Chandrasekaran C, Goo W, Diester I, Ramakrishnan C, Kaufman MT, Ryu SI, Yeom KW, Deisseroth K, Shenoy KV, 2018 Development of an optogenetic toolkit for neural circuit dissection in squirrel monkeys. Sci. Rep. 8, 1–20. 10.1038/s41598-018-24362-7 [PubMed: 29311619]

Paxinos G, Huang X, Toga AW, 2000 The Rhesus Monkey Brain in Stereotaxic Coordinates. San Diego, USA: Academic Press

Peterchev AV, Jalinous R, Lisanby SH, 2008 A transcranial magnetic stimulator inducing near-rectangular pulses with controllable pulse width (cTMS). IEEE Trans. Biomed. Eng 55, 257–266. 10.1109/TBME.2007.900540 [PubMed: 18232369]

Peterchev AV, Krystal AD, Rosa MA, Lisanby SH, 2015 Individualized Low-Amplitude Seizure Therapy: Minimizing Current for Electroconvulsive Therapy and Magnetic Seizure Therapy. Neuropsychopharmacology 40, 2076–2084. 10.1038/npp.2015.122 [PubMed: 25920013]

Pillay S, Meyer NL, Puschnik AS, Davulcu O, Diep J, Ishikawa Y, Jae LT, Wosen JE, Nagamine CM, Chapman MS, Carette JE, 2016 An essential receptor for adeno-associated virus infection. Nature 530, 108–112. 10.1038/nature16465 [PubMed: 26814968]

Preston RJ, Bishop GA, Kitai ST, 1980 Medium spiny neuron projection from the rat striatum: An intracellular horseradish peroxidase study. Brain Res. 183, 253–263. 10.1016/0006-8993(80)90462-X [PubMed: 7353139]

Raper J, Murphy L, Richardson R, Romm Z, Kovacs-Balint Z, Payne C, Galvan A, 2019 Chemogenetic inhibition of the amygdala modulates emotional behavior expression in infant rhesus monkeys. eNeuro 6 10.1523/ENEURO.0360-19.2019

Ren J, Friedmann D, Xiong J, Liu CD, Ferguson BR, Weerakkody T, DeLoach KE, Ran C, Pun A, Sun Y, Weissbourd B, Neve RL, Huguenard J, Horowitz MA, Luo L, 2018 Anatomically Defined and Functionally Distinct Dorsal Raphe Serotonin Sub-systems. Cell 175, 472–487.e20. 10.1016/j.cell.2018.07.043 [PubMed: 30146164]

Salegio EA, Samaranch L, Kells AP, Mittermeyer G, San Sebastian W, Zhou S, Beyer J, Forsayeth J, Bankiewicz KS, 2013 Axonal transport of adeno-associated viral vectors is serotype-dependent. Gene Ther. 20, 348–352. 10.1038/gt.2012.27 [PubMed: 22418061]

Samulski RJ, Chang LS, Shenk T, 1989 Helper-free stocks of recombinant adeno-associated viruses: normal integration does not require viral gene expression. J. Virol 63, 3822–3828. 10.1128/jvi.63.9.3822-3828.1989 [PubMed: 2547998]

San Sebastian W, Samaranch L, Heller G, Kells AP, Bringas J, Pivirotto P, Forsayeth J, Bankiewicz KS, 2013 Adeno-associated virus type 6 is retrogradely transported in the non-human primate brain. Gene Ther. 20, 1178–1183. 10.1038/gt.2013.48 [PubMed: 24067867]

Sato TK, Häusser M, Carandini M, 2013 Distal connectivity causes summation and division across mouse visual cortex. Nat. Publ. Gr 17 10.1038/nn.3585

Senova S, Poupon C, Dauguet J, Stewart HJ, Dugué GP, Jan C, Hosomi K, Ralph GS, Barnes L, Drouot X, Pouzat C, Mangin JF, Pain F, Doignon I, Aron-Badin R, Brouillet E, Boyden ES, Mitrophanous KA, Hantraye P, Palfi S, 2018a Optogenetic Tractography for anatomo-functional characterization of cortico-subcortical neural circuits in non-human primates. Sci. Rep 8, 1–12. 10.1038/s41598-018-21486-8 [PubMed: 29311619]

Simonelli F, Maguire AM, Testa F, Pierce EA, Mingozzi F, Bennicelli JL, Rossi S, Marshall K, Banfi S, Surace EM, Sun J, Redmond TM, Zhu X, Shindler KS, Ying GS, Ziviello C, Acerra C, Wright JF, McDonnell JW, High KA, Bennett J, Auricchio A, 2010 Gene therapy for leber's congenital amaurosis is safe and effective through 1.5 years after vector administration. Mol. Ther 18, 643–650. 10.1038/mt.2009.277 [PubMed: 19953081]

Schnell MJ, McGettigan JP, Wirblich C, Papaneri A, 2010 The cell biology of rabies virus: Using stealth to reach the brain. Nat. Rev. Microbiol 10.1038/nrmicro2260

Soudais C, Laplace-Builhe C, Kissa K, Kremer EJ, 2001 Preferential transduction of neurons by canine adenovirus vectors and their efficient retrograde transport in vivo. FASEB J. 15, 2283–2285. 10.1096/fj.01-0321fje [PubMed: 11511531]

Stanton GB, Goldberg ME, Bruce CJ, 1988A Frontal eye field efferents in the macaque monkey: I. Subcortical pathways and topography of striatal and thalamic terminal fields. J. Comp. Neurol 271, 473–492. 10.1002/cne.902710402 [PubMed: 2454970]

Stanton GB, Goldberg ME, Bruce CJ. 1988B Frontal eye field efferents in the macaque monkey: II. Topography of terminal fields in midbrain and pons. J Comp Neurol271(4):493–506. [PubMed: 2454971]

Stauffer WR, Lak A, Yang A, Borel M, Paulsen O, Boyden ES, Schultz W, 2016 Dopamine Neuron-Specific Optogenetic Stimulation in Rhesus Macaques. Cell 166, 1564–1571.e6. 10.1016/j.cell.2016.08.024 [PubMed: 27610576]

Sun L, Tang Y, Yan K, Yu J, Zou Y, Xu W, Xiao K, Zhang Z, Li W, Wu B, Hu Z, Chen K, Fu ZF, Dai J, Cao G, 2019a Differences in neurotropism and neurotoxicity among retrograde viral tracers. Mol. Neurodegener 14 10.1186/s13024-019-0308-6

Takada M, Inoue K-I, Koketsu D, Kato S, Kobayashi K, Nambu A, 2013 Elucidating information processing in primate basal ganglia circuitry: a novel technique for pathway-selective ablation mediated by immunotoxin. Front. Neural Circuits 7, 140 10.3389/fncir.2013.00140 [PubMed: 24027499]

Takada M, Tokuno H, Hamada I, Inase M, Ito Y, Imanishi M, Hasegawa N, Akazawa T, Hatanaka N, Nambu A, 2001 Organization of inputs from cingulate motor areas to basal ganglia in macaque monkey. Eur. J. Neurosci 14, 1633–1650. 10.1046/j.0953-816X.2001.01789.x [PubMed: 11860458]

Tamura K, Takeda M, Setsuie R, Tsubota T, Hirabayashi T, Miyamoto K, Miyashita Y, 2017 Conversion of object identity to object-general semantic value in the primate temporal cortex. Science (80-.). 357, 687–692. 10.1126/science.aan4800

Tanabe S, Inoue K. ichi, Tsuge H, Uezono S, Nagaya K, Fujiwara M, Kato S, Kobayashi K, Takada M, 2017 The use of an optimized chimeric envelope glycoprotein enhances the efficiency of retrograde gene transfer of a pseudotyped lentiviral vector in the primate brain. Neurosci. Res 120, 45–52. 10.1016/j.neures.2017.02.007 [PubMed: 28257798]

Tanabe S, Uezono S, Tsuge H, Fujiwara M, Miwa M, Kato S, Nakamura K, Kobayashi K, Inoue K. ichi, Takada M, 2019 A note on retrograde gene transfer efficiency and inflammatory response of lentiviral vectors pseudotyped with FuG-E vs. FuG-B2 glycoproteins. Sci. Rep 9, 1–12. 10.1038/s41598-019-39535-1 [PubMed: 30626917]

Taymans JM, Vandenberghe LH, Van Den Haute C, Thiry I, Deroose CM, Mortelmans L, Wilson JM, Debyser Z, Baekelandt V, 2007 Comparative analysis of adeno-associated viral vector serotypes 1, 2, 5, 7, and 8 in mouse brain. Hum. Gene Ther 18, 195–206. 10.1089/hum.2006.178 [PubMed: 17343566]

Tervo DGR, Hwang BY, Viswanathan S, Gaj T, Lavzin M, Ritola KD, Lindo S, Michael S, Kuleshova E, Ojala D, Huang CC, Gerfen CR, Schiller J, Dudman JT, Hantman AW, Looger LL, Schaffer DV, Karpova AY, 2016 A Designer AAV Variant Permits Efficient Retrograde Access to Projection Neurons. Neuron 92, 372–382. 10.1016/j.neuron.2016.09.021 [PubMed: 27720486]

Tohyama T, Kinoshita M, Kobayashi Kenta, Isa K, Watanabe D, Kobayashi Kazuto, Liu M, Isa T, Strick PL, 2017 Contribution of propriospinal neurons to recovery of hand dexterity after corticospinal tract lesions in monkeys. Proc. Natl. Acad. Sci. U. S. A 114, 604–609. 10.1073/pnas.1610787114 [PubMed: 28049844]

Towne C, Schneider BL, Kieran D, Redmond DE, Aebischer P, 2010 Efficient transduction of non-human primate motor neurons after intramuscular delivery of recombinant AAV serotype 6. Gene Ther. 17, 141–146. 10.1038/gt.2009.119 [PubMed: 19727139]

Tsiang H, 1979 Evidence for an intraaxonal transport of fixed and street rabies virus. J. Neuropathol. Exp. Neurol 38, 286–296. 10.1097/00005072-197905000-00008 [PubMed: 86604]

Upright NA, Brookshire SW, Schnebelen W, Damatac CG, Hof PR, Browning PGF, Croxson PL, Rudebeck PH, Baxter MG, 2018 Behavioral Effect of Chemogenetic Inhibition Is Directly Related to Receptor Transduction Levels in Rhesus Monkeys. J. Neurosci 38, 7969–7975. 10.1523/jneurosci.1422-18.2018 [PubMed: 30082415]

Wang X, Zhang C, Szábo G, Sun QQ, 2013 Distribution of CaMKIIα expression in the brain in vivo, studied by CaMKIIα-GFP mice. Brain Res. 1518, 9–25. 10.1016/j.brainres.2013.04.042 [PubMed: 23632380]

Wang Z, Maunze B, Wang Y, Tsoulfas P, Blackmore MG, 2018 Global connectivity and function of descending spinal input revealed by 3D microscopy and retrograde transduction. J. Neurosci 38, 10566–10581. 10.1523/JNEUROSCI.1196-18.2018 [PubMed: 30341180]

Watakabe A, Ohtsuka M, Kinoshita M, Takaji M, Isa K, Mizukami H, Ozawa K, Isa T, Yamamori T, 2015 Comparative analyses of adeno-associated viral vector serotypes 1, 2, 5, 8 and 9 in marmoset, mouse and macaque cerebral cortex. Neurosci. Res 93, 144–157. 10.1016/j.neures.2014.09.002 [PubMed: 25240284]

Weiss AR, Liguore WA, Domire JS, Button D, McBride JL, 2020. Intra-striatal AAV2.retro administration leads to extensive retrograde transport in the rhesus macaque brain: implications for disease modeling and therapeutic development. Sci. Rep 10, 1–14. 10.1038/s41598-020-63559-7 [PubMed: 31913322]

Wu SH, Liao ZX, D Rizak J, Zheng N, Zhang LH, Tang H, He X. Bin, Wu Y, He XP, Yang MF, Li ZH, Qin DD, Hu XT, 2017 Comparative study of the transfection efficiency of commonly used viral vectors in rhesus monkey (Macaca mulatta) brains. Zool. Res 38, 88–95. 10.24272/j.issn.2095-8137.2017.015 [PubMed: 28409504]

Yaguchi M, Ohashi Y, Tsubota T, Sato A, Koyano KW, Wang N, Miyashita Y, 2013 Characterization of the properties of seven promoters in the motor cortex of rats and monkeys after lentiviral vector-mediated gene transfer. Hum. Gene Ther. Methods 24, 333–344. 10.1089/hgtb.2012.238 [PubMed: 23964981]

Yazdan-Shahmorad A, Diaz-Botia C, Hanson TL, Kharazia V, Ledochowitsch P, Maharbiz MM, Sabes PN, 2016 A Large-Scale Interface for Optogenetic Stimulation and Recording in Nonhuman Primates. Neuron 89, 927–939. 10.1016/j.neuron.2016.01.013 [PubMed: 26875625]

Yazdan-Shahmorad A, Tian N, Kharazia V, Samaranch L, Kells A, Bringas J, He J, Bankiewicz K, Sabes PN, 2018 Widespread optogenetic expression in macaque cortex obtained with MR-guided, convection enhanced delivery (CED) of AAV vector to the thalamus. J. Neurosci. Methods 293, 347–358. 10.1016/j.jneumeth.2017.10.009 [PubMed: 29042259]

Yeterian EH, Van Hoesen GW, 1978 Cortico-striate projections in the rhesus monkey: The organization of certain cortico-caudate connections. Brain Res. 139, 43–63. 10.1016/0006-8993(78)90059-8 [PubMed: 413609]

Zheng N, Wang Z, Wang S, Yang F, Zhu X, Lu C, Manyande A, 2020 Co-localization of two-color rAAV2-retro confirms the dispersion characteristics of efferent projections of mitral cells in mouse accessory olfactory bulb 41, 1–9. 10.24272/j.issn.2095-8137.2020.020

Zingg B, Chou X. lin, Zhang Z. gang, Mesik L, Liang F, Tao HW, Zhang LI, 2017 AAV-Mediated Anterograde Transsynaptic Tagging: Mapping Corticocollicular Input-Defined Neural Pathways for Defense Behaviors. Neuron 93, 33–47. 10.1016/j.neuron.2016.11.045 [PubMed: 27989459]

HIGHLIGHTS

When injected into rhesus macaque striatal and oculomotor structures, rAAV2-retro:

- Produces robust retrograde labeling in most structures with direct projections to the injection site, likely sufficient for circuit manipulation in rhesus macaque opto- and chemogenetic studies
- Does not retrogradely label *all* structures with direct projections to the injection site
- Produces robust terminal field labeling in many structures that receive direct projections from the injection site

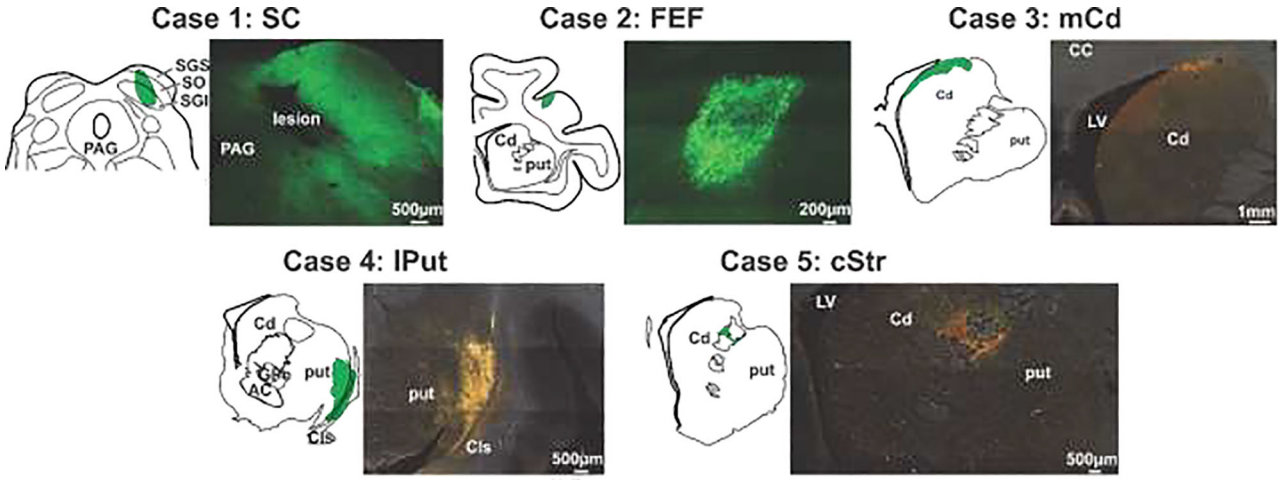

Figure 1. Injection sites.

An illustration and image are shown to demonstrate the injection site location in each case. The extent of the injection site in each case is shown in green in the illustration. AC= anterior commissure; CC= corpus callosum; Cd=caudate; Cls=claustrum; cStr=central striatum; FEF=frontal eye field; GPe= globus pallidus, external segment; lPut=lateral putamen; LV=lateral ventricle; mCd=medial caudate; PAG=periaqueductal gray; put=putamen; SC=superior colliculus; SGl=stratum griseum intermedium; SGS=stratum griseum superficiale; SO=stratum opticum;.

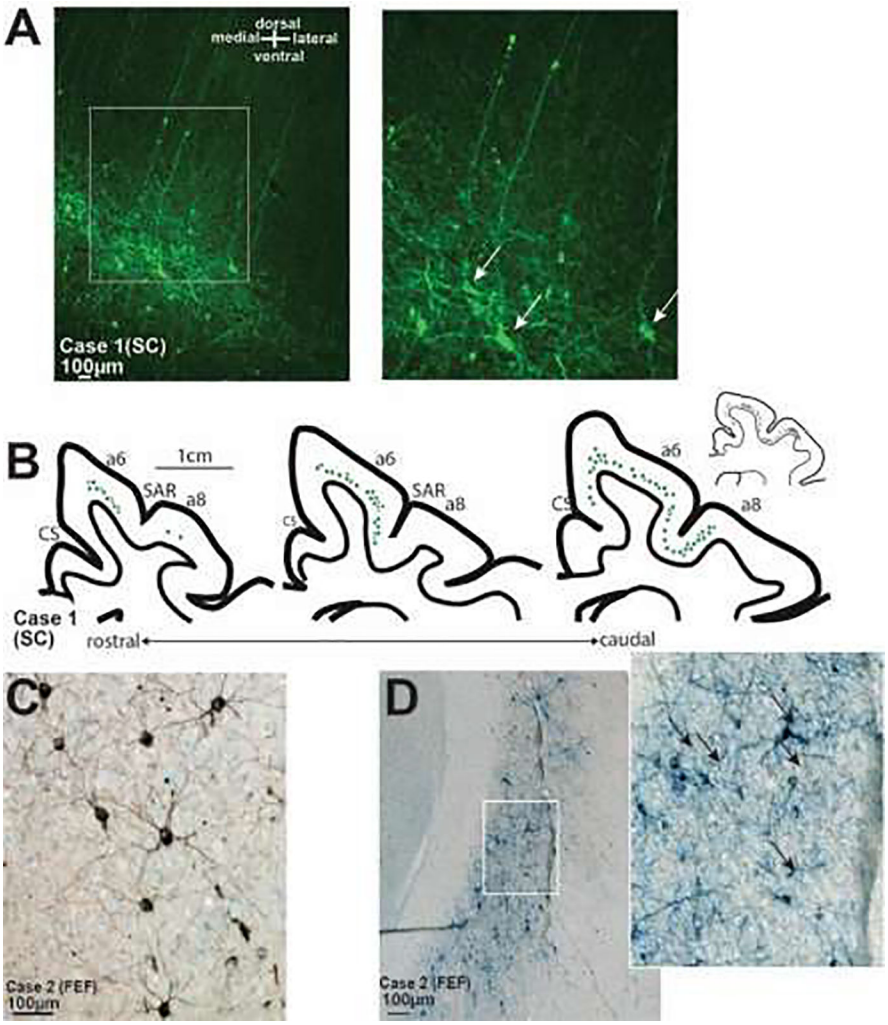

Figure 2. Retrograde labeling in visuomotor circuitry.

A-B. Following rAAV2-retro injections into the superior colliculus (SC) (Case 1), dense retrograde labeling was observed in the frontal eye field (FEF). (**A**) shows a low magnification view of FEF on the left. The boxed area is shown at higher magnification on the right. Labeled pyramidal cell somata are indicated by arrows. Note the extensive dendritic labeling. (**B**) shows chartings of cortical retrograde labeling (green dots) following rAAV2-retro injections in SC. Only labeling in the FEF and immediate vicinity is shown. Inset in (**B**) shows cortical labeling in the FEF and immediate vicinity following an injection of a classical tract-tracer, horseradish peroxidase, into the SC (adapted with permission from Leichnetz et al., 1981). **C-D.** Following rAAV2-retro injections into FEF (Case 2), dense retrograde labeling was observed in the contralateral FEF (**C**) and ipsilateral claustrum (**D**). The box in D (left plate) indicates the region shown at higher magnification in the right plate, where labeled cells are indicated by arrows. a6=area 6; a8=area 8; CS=cingulate sulcus; FEF=frontal eye field; SAR=superior arcuate sulcus; SC=superior colliculus.

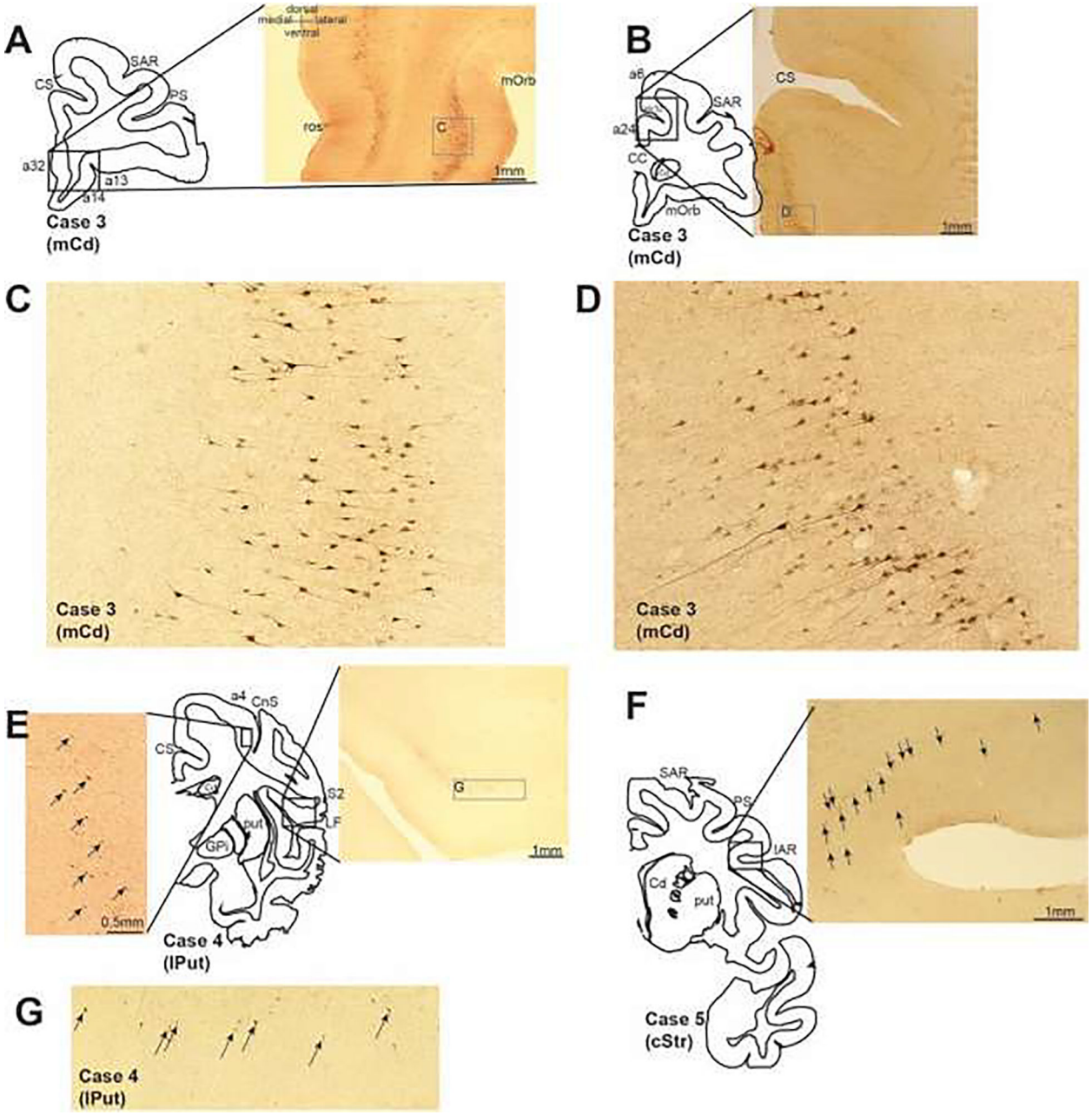

Figure 3. Retrograde labeling in cortico-basal ganglia circuitry.

Selected examples of cortical labeling following rAAV2-retro injections into striatum. Following injections into the medial caudate nucleus (Case 3), dense retrograde labeling was observed in the ventromedial prefrontal and medial orbitofrontal cortices (**A**&**C**) and the dorsal anterior cingulate cortex (**B**&**D**). The boxed areas in the photomicrographs in (**A**&**B)** are shown at higher magnification in (**C**&**D)**, respectively. Note the extensive dendritic labeling. Following injections into the ventrolateral putamen (Case 4), significant retrograde labeling was observed in the sensorimotor cortices (**E**). The boxed region shown in the left photomicrograph in (**E**) is located in primary motor cortex. The boxed region shown on the right in (**E**) is located in the secondary somatosensory cortex. In both cases, brown, labeled

cells are indicated by arrows. Following injections into the dorsocentral striatum (Case 5), retrograde labeling was observed in the lateral prefrontal cortices (**F**). Arrows indicate a row of brown, labeled cells in layer V. **G.** Enlargement of the boxed region in the secondary somatosensory cortex from (**E**). a4=area 4; a13=area 13; a14=area 14; a24=area 24; a32=area 32; CC=corpus callosum; Cd=caudate nucleus; CS=cingulate culcus; CnS=central sulcus; cStr=central striatum; GPi=globus pallidus, internal segment; IAR=inferior arcuate sulcus; LF=lateral fissure; lPut=lateral putamen; mCd=medial caudate nucleus; mOrb=medial orbital sulcus; PS=principal sulcus; put=putamen; ros=rostral sulcus; SAR=superior arcuate sulcus.

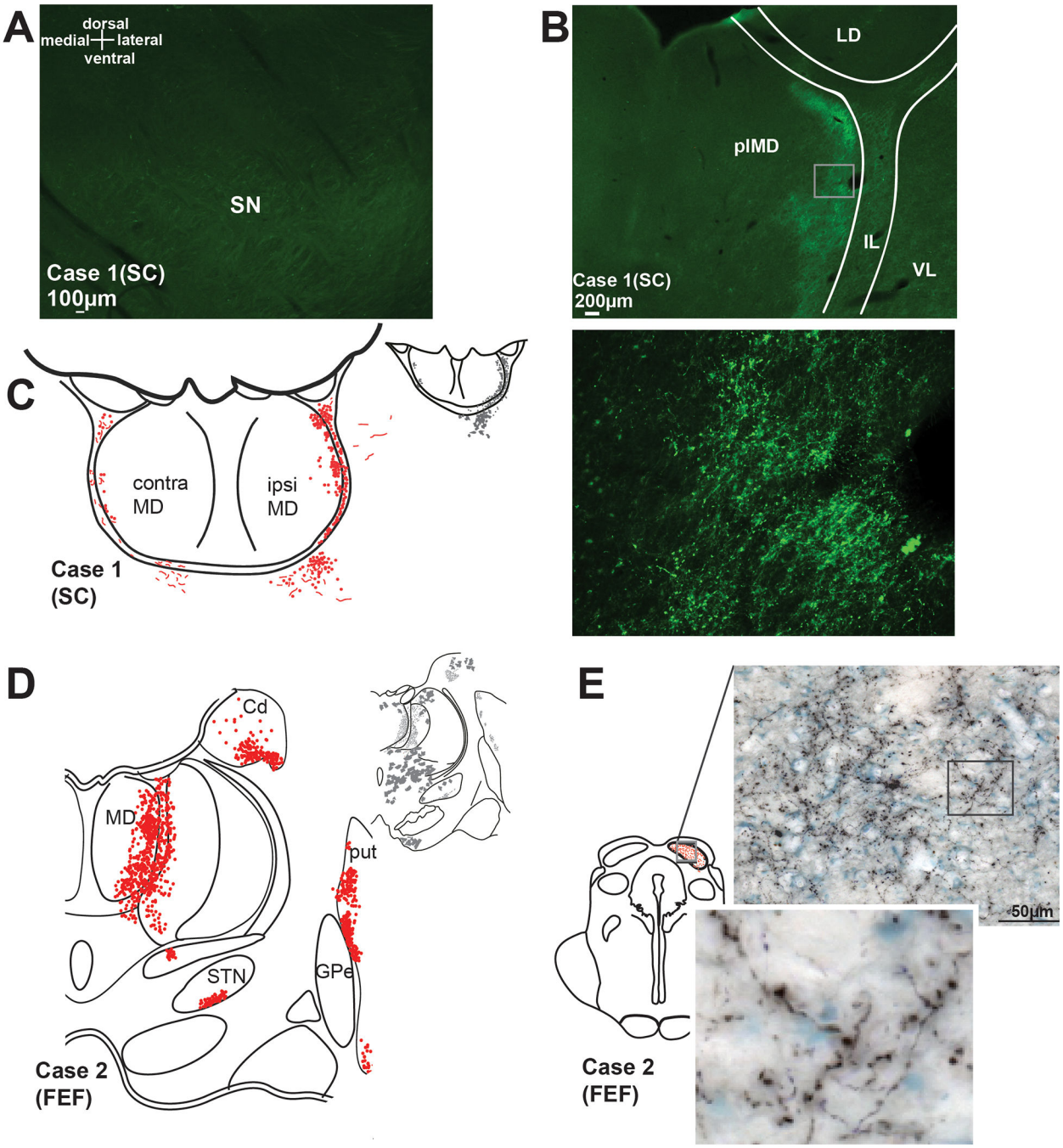

Figure 4. Additional characterization of labeling in visuomotor circuitry: false negatives and terminal fields.

rAAV2-retro injections into SC (Case 1) should result in retrograde labeling in the substantia nigra pars reticulata, but no labeled cells were observed (**A**). Photomicrographs (**B**) and a charting (**C**) indicate the pattern of terminal field labeling in the thalamus following rAAV2-retro injections in SC (Case 1). A dense terminal field is present in the paralamellar portion of the mediodorsal nucleus of the thalamus (**B**). The box in the upper plate is shown at higher magnification in the lower plate to demonstrate the labeling of individual terminal

puncta. The charting in (**C**) shows the pattern of terminal label (red stipple) in the ipsilateral and contralateral mediodorsal nucleus of the thalamus, and the adjacent intralaminar zones. For comparison, inset in (**C**) shows terminal field labeling from a case in which the conventional anterograde tract-tracer WGA-HRP was injected into the SC (adapted with permission from May, 2006). (**D**) shows charting of terminal field labeling (red stipple) in the thalamus and basal ganglia following rAAV2-retro injections in FEF (Case 2). Terminal fields were located laterally in mediodorsal nucleus of the thalamus and the adjacent intralaminar zone, as well as in the caudate, putamen and subthalamic nucleus. For comparison, inset in (**D**) shows terminal field labeling from a case in which a traditional anterograde tract-tracer, tritiated amino acids, was injected into FEF (adapted with permission from Stanton et al., 1988). Charting in (**E**) shows the pattern of terminal labeling (red stipple) in the deeper layers of the SC following rAAV2-retro injections into FEF. The density of the terminal field can be appreciated in the upper photomicrograph. The boxed region, shown at higher magnification in the lower plate, reveals the morphology of the axonal arbors. Cd =caudate nucleus; contra=contralateral to the injection site; FEF=frontal eye field; GPe=globus pallidus, external segment; IL=internal medullary laminae; ipsi=ipsilateral to the injection site; LD=lateral dorsal nucleus of the thalamus; MD=mediodorsal nucleus of the thalamus; PAG=periaqueductal gray; plMD=paralamellar mediodorsal nucleus of the thalamus; put=putamen; SC=superior colliculus; STN=subthalamic nucleus; VL=ventral lateral nucleus of the thalamus.

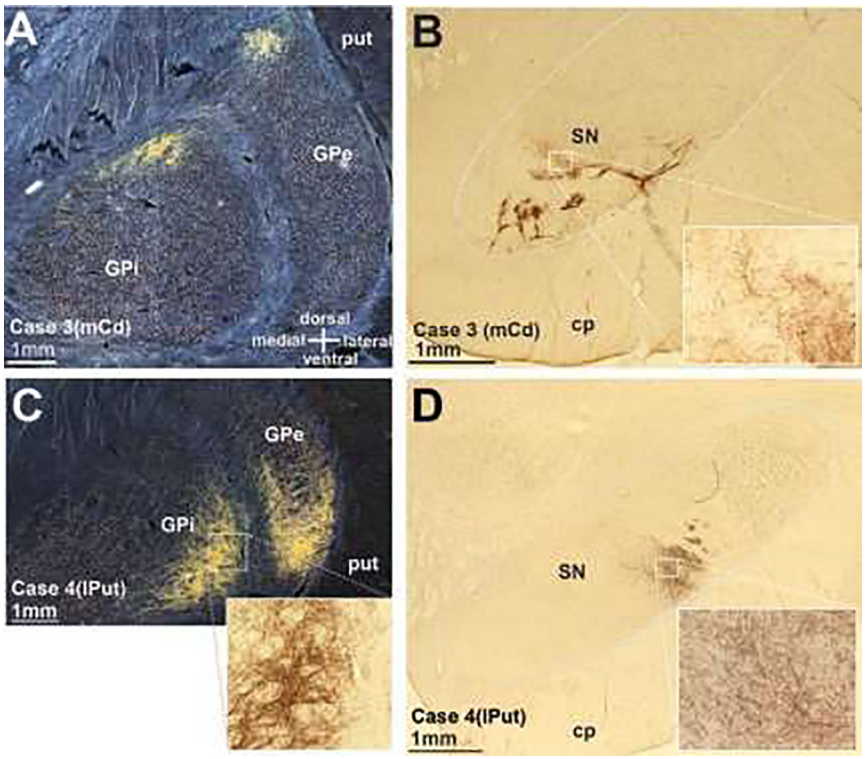

Figure 5. Additional characterization of labeling in cortico-basal ganglia circuitry: false negatives and terminal fields.

rAAV2-retro injections in the dorsomedial caudate (Case 3) resulted in terminal field labeling in both segments of the pallidum (**A**), shown with dark field illumination, and in the medial part of the substantia nigra (likely involving both the pars compacta and pars reticulata) (**B**). The box in (**B**) is shown at higher magnification in the inset. rAAV2-retro injections in the ventrolateral putamen (Case 4) resulted in terminal field labeling, but not retrograde labeling, in both segments of the pallidum (**C**), shown with dark field illumination, and in a more lateral part of the substantia nigra (likely involving both the pars compacta and pars reticulata) (**D**). Boxed regions in both (**C)** and (**D)** are shown at higher magnification in the insets. cp=cerebral peduncle; GPe=globus pallidus, external segment; GPi=globus pallidus, internal segment; put=putamen; mCd=medial caudate; SN=substantia nigra.

Table 1:

Cases in this study.

Subject ID	Case #	Injection location	Viral construct	Source	Transport time (days)	Titer	Volume injected (μl)	Injection rate (μl/min)	# of tracks/ # of injections per track/ spacing between injections in each track (mm)
M18-11	**1**	SC	rAAV2-retro-hSyn-hChR2(H134R)-EYFP	Salk Institute Viral Vector Core	264	2.5×10^{13}	9	0.1	3/3/0.5
M17-04	**2**	FEF	rAAV2-retro-CAG-GFP	University of North Carolina Vector Core	28	1.8×10^{12}	18	1	6/2/1
M15	**3**	mCd	rAAV2-retro-CaMKII - hM4Di-mCherry	University of Minnesota Viral Vector & Cloning Core	48	1.2×10^{14}	25	1	1/1/--
M15	**4**	lPut	rAAV2-retro-hSyn-hM4Di-HA	University of Minnesota Viral Vector & Cloning Core	48	1.3×10^{14}	25	1	1/2/2
M11	**5**	cStr	rAAV2-retro-CaMKII-hM4Di-mCherry	University of Minnesota Viral Vector & Cloning Core	56	1.2×10^{14}	18	0.5	1/2/2.3

Transport time is time between injection and sacrifice. Titer given in GC/ml (Cases 3–5) or pp/ml (Cases 1–2). cStr=central striatum; FEF=frontal eye fields; lPut=lateral putamen; mCd=medial caudate; SC=superior colliculus.